Finite Element Analysis and Preliminary Experiments to Study the Effects of High Myopia in Macular Degeneration

A Thesis presented

by

Aneesh Ajay Bendre

to

Department of Mechanical and Industrial Engineering

In partial fulfillment of the requirements for the degree of

Master of Science

In the field of
Mechanics

Northeastern University
Boston, Massachusetts
August 2009.

Acknowledgements

I would like to express my sincere gratitude to my advisor, Professor George G. Adams who advised and motivated me during my research work. Most importantly for bringing up the topic and also had been there always for those invaluable discussions. Though the field of biomechanics was new to me, his enthusiasm, his inspiration and his efforts to explain the concepts in a simple and practical manner helped me in understanding and then contributing in my research work. I would also like to thank Professors K-T Wan and Jeffrey W. Ruberti for their advice and guidance in this work. I would like to express my gratitude towards Mechanical and Industrial engineering department for giving me the opportunity to pursue my Masters program. I would like to thank my fellow graduate students Hassan, Edgar and Ramin for their support during this research. Last but not the least, sincere appreciation to all my family and friends who had been there to encourage and help during the tough times of this study

ABSTRACT

Axial myopia is characterized by an elongation of the eye and defocusing of the image formed on the macula (central retina). The elongation in high myopia stretches the retina, which can cause hemorrhage, atrophy and the formation of new blood vessels in the macula and underlying tissue. This process leads to scarring, blurring and even loss of useful central vision.

A modeling approach has been developed to study the effect of deformed geometry, material properties and intraocular pressure on the pathology of myopic macular degeneration. 2-D axisymmetric and three dimensional finite element models of a myopic eye were generated to study the induced stress and integrity of the retinal layers. Cases of linear, bilinear and hyper-elastic Mooney-Rivlin material behavior were examined for the retina and linear and hyper-elastic Ogden (n=1) material model for the choroid. Mechanical tests were performed to mechanical material properties of bovine choroid membrane along with a traditional uniaxial tensile test. The modulus of elasticity for the bovine choroid averaged 0.2 ± 0.08 MPa. Direct measurements enable the use of more realistic material properties during modeling. The finite element models showed maximum radial and circumferential stress in the region of the macula in each model. Maximum radial and circumferential tensile strains of 11% were observed in the macular region. Such high strains indicate that this region would be most vulnerable to mechanical changes occurring in axial myopia. Increased tensile strain (stretching of the retina) could lead to reduction of the density of photoreceptor cells, hemorrhage and formation of cracks in the macular region making it favorable for new blood vessels to grow in this region. Formation of these vessels can lead to bleeding; the result of which is scarring and loss of vision.

Thus the finite element modeling proves to be an effective method to study the mechanics involved in axial myopia, providing a mechanical explanation for the pathology of myopic macular degeneration.

TABLE OF CONTENTS

LIST OF FIGURES

LIST OF TABLES

1. Introduction

The Macula is the central region of the retina which is responsible for high acuity vision. Visual acuity enables us to see sharp, detailed image making tasks such as reading, driving and face recognition possible. Myopia is one of the leading causes of affected vision. It is characterized by blurred vision and near sightedness. Elongation of the eye ball is noted as the cause in patients with myopia. Myopia is caused by genetic as well as environmental factors. Progressive myopia can lead to Macular Degeneration (MD)[1]. Degenerative changes include retinal layer atrophy, neo-vascularization, lesion formation and retinal detachment. These changes affect central vision, causes blurring of central image and the occurrence of dark spots. Even though 100% vision loss is not observed, affected vision decreases efficiency and hampers routine life of patients. Another type of macular degeneration affecting a significant number of elderly population is Age Related Macular Degeneration (AMD).

Amsler Grid is used for primary detection of macular degeneration. Progression of Macular Degeneration has been extensively studied through clinical trials [2]. However, effective treatment is not yet commercially available making it difficult to prevent and predict the onset of the disease. Mechanical factors have been implicated in the degenerations observed in MD. Elongations of the eye ball, material properties of retinal layers and intraocular pressure (IOP) changes have previously been studied. Bell[1] discussed the changes that occur in the sclera, choroid and retina and their contribution to high myopia. Friedman [3] has applied Laplace's law to the eye to calculate the stress in the sclera. Greene[4] has also studied the mechanics of the myopic eye by applying Laplace's law to calculate stress in the sclera and compared the Optic disc to a 'hole in a plate problem'. Greene used results of parallel forces acting on plates to compare the stress due to external muscles on the eye. In another study, Greene [5] applied the theories of stress amplification of spheroid shells to the myopic eye. Perkins [6] applied the Laplace's law to calculate the scleral stress by measuring axial length, IOP and scleral thickness. However, he could not provide a substantial relation between myopia and mechanical stress. Balloon expansion characteristics have been applied to fluid filled rubber balls to compare them to the myopic eye [7]. However visco-elastic effects of the sclera had not been taken into effect before directly applying such theories. Mechanical analysis for the

possible explanation of choroidal folds was provided by Friberg [8]. Friberg explained the choroidal folds using principles of deformation of materials.

Finite Element (FE) Modeling has been previously used to study the mechanics of the eye. Springer *et al* [9] modeled the macular region to study the development of the fovea. They used non-linear Mooney-Rivlin properties for the retina only. Other layers of the eye like the choroid and the sclera have not been modeled. Sigal *et al* [10], [11] and Bellazza *et al* [12] have created detailed FE models of the optic disc to study glaucoma using linear elastic material properties. Ljubimova *et al* [13] have studied accommodation in the eye and their FE model included the lens, zonules and vitreous humor of the eye using linear elastic material properties. They established their modeling results to be reasonable and supporting the Helmholtz [14, 15] theory of accommodation.

The contribution of mechanical factors has been observed in the clinical trial undertaken to study the pathogenesis of Myopia. Klein *et al* [16] noted that the lacquer cracks in high myopia represent healed mechanical breaks in the Retinal pigment Epithelium (RPE), Bruch's membrane and chorio-capillaries. A mechanical theory was postulated [16] that degeneration followed the retinal stretching caused by an increase in axial length. Shapiro's [17] clinical findings supported this mechanical hypothesis for the changes in the myopic eye. Over a nine year period the axial length of a subject increased by 1.3 mm in right eye and 3.1 mm in left eye. Along with this increase, lacquer cracks appeared secondary to stretching of the eyeball. Subretinal hemorrhage also occurred at locations where lacquer cracks subsequently appeared.

This study aims to analyze the effect of varying mechanical parameters on the behavior of the retinal layers of the myopic eye. Finite Element Analysis is utilized as a modern tool in engineering analysis of biological samples. This method enabled modeling of the myopic eye, comparison of different materials, its behavior at varying intra-ocular pressures in detail and in a time efficient manner. Previous studies used linear elastic material properties for studying eye models [10, 12]. Springer *et al* [9] did not take into consideration the geometry of the entire eye. This study is a novel approach to quantify the stress on the retinal layer due to high

myopia. The effect of varying material properties and IOP will be analyzed to calculate maximum stress value which could be critical to predict degenerative changes in myopic eye.

The FEM models of the retina in high myopia that were generated are consistent, repeatable and scalable. Construction of these models was based on the hypothesis that the retina tries to conform to the elongated sclera. This effort of the retina would cause excessive stress perhaps making it vulnerable to atrophy. Experimentation using bovine eyes was carried out with the aim of comparing the experimental choroid material values with that in the literature. Tensile and membrane tests were performed to study the material properties of a bovine choroid. We aim to quantify the critical parameters that induce conditions favorable for myopic macular degeneration.

2. Background information

Brief anatomy
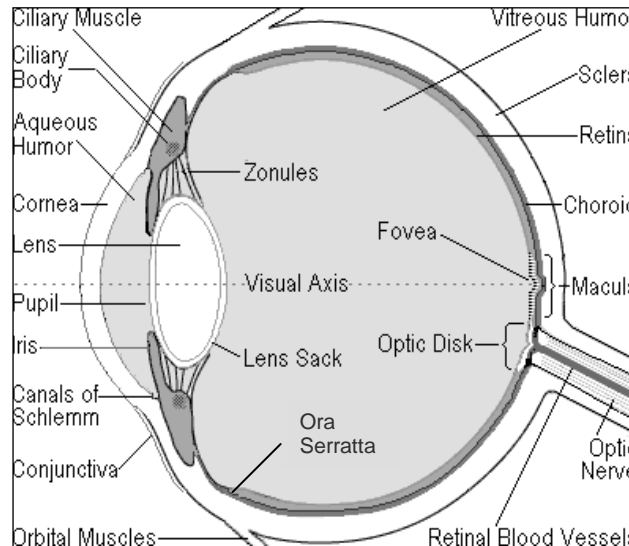
Fig.1. Cross section of the eye.

http://www.99main.com/~charlief/Blindness.hm#vxa

The eye is comprised of two sections of spherical shells, Fig.1. The anterior corneal shell (radius 7.8mm) consists of the cornea and the aqueous humor, while the posterior scleral shell (radius 12mm) consists of retina, choroid, sclera, vitreous humor and optic disc. The cornea is a transparent layer that covers the anterior part of the eye. The aqueous humor is a transparent fluid that fills the corneal shell. The lens (diameter 10mm, central thickness 4mm) is situated between the corneal and scleral shells. It is held in position by zonules and ciliary muscles.

Table 1 : Dimensions of the human eye[18].

Human Eye	Axial length 24mm, vertical 23mm,horizontal diameter 23.5mm
Retina	Surface area: 266mm^2, thickest at 0.56mm
Fovea	1.85mm diameter, 0.25mm thickness
Sclera	0.6mm at the equator, radius 12mm
Choroid	220µm in the macular region
Macula	3mm diameter,
Cornea	0.52mm axial thickness, radius 7.8mm
Optic Disc	Area 2.69mm^2, disc width 1.76mm, vertical 1.92mm

The sclera is the outermost layer of the scleral shell. The retina spreads over the inner part of the sclera. The retina acts as the screen of the eye. The retina is attached to the ora serratta at its periphery. The neuro-sensory rods and cones present on the retina act as photoreceptors. The center of the retina is known as macula. The fovea is a pit at the center of macula. The choroid lies between the retina and the sclera. The optic disc, located near the fovea, is the region where the optic nerve connects to the retina. The optic nerve transmits the light stimuli to the brain. The vitreous humor occupies the region between the lens and the retina and helps maintain the retina in its position. The dimensions of the eye are given in Table 1.

Visual function

The cornea acts as a protective outermost anterior layer of the eye. The lens along with the cornea refracts the light onto the retina. The ciliary muscles help to contract the lens. This allows the eye to adjust the focal length to view objects at different distances. The aqueous humor provides nourishment to the cornea and the lens. The rods on the retina are responsible for vision at low light level while the cones are responsible for vision at high light levels. There is a high density of cones in the fovea region averaging 199,000 cones/mm^2.[18] This region is hence characterized by high visual acuity. Visual Acuity is the sharpness or clearness of vision. It is measured in Snellen Fractions typically 20/20, 20/40 and so on. The Snellen Fraction for an eye represents the ratio of the distances needed to see an object by standard vision to that by affected vision. If a person sees 20/40, at 20 feet from the chart that person can read letters that a person with 20/20 vision could read from 40 feet away.

Retina

The retina consists of three layers of nerve cells, Fig. 2. The outermost layer of the retina is formed of rods and cones. These are activated by the light stimuli and hence are called photoreceptors. Once stimulated, the rods and cones transmit the signal to the ganglion cells through the bipolar cell layer. The plexiform located in between two adjacent nerve cell layers is the region of synaptic contact. Information flows from one neuron to the other across this synapse. The signal is further carried by the nerve fiber layer to the optic nerve and finally to the brain.
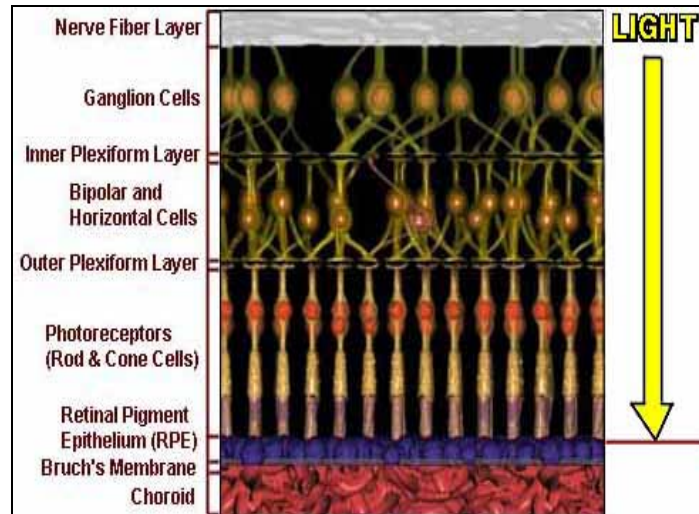
Fig. 2. Cross section of the retina.

www.mdsupport.org

Macula

The macula region of the retina has a distinct histological structure. Its periphery is marked by a single layer of ganglion cells. This region is void of retinal blood vessels. The high acuity of vision is possible because of the large concentration of cones in the macula.

Fovea

The central region of the macula has a depression or pit known as the fovea. The photoreceptor layer in this area consists of only cones. The inner nuclear layer is reduced in thickness at the edge of the fovea and is absent within the foveal pit. The internal plexiform, ganglion cell and nerve fiber layer are also absent in the fovea. The retinal blood vessels are mostly capillaries running only up to the edge of the fovea. The capillary free area in the macula is about 0.4 mm in diameter.

The cones in the foveal pit obtain nourishment with the help of the retinal pigment epithelium cells (RPE). The RPE and Bruch's membrane are situated in between the retina and the choroid. The Bruch's membrane consists of collagen and a thin basal membrane.

Retinal and choroidal blood supply

The inner retina is supplied with blood by the retinal artery. The retinal artery runs along the optic nerve and branches out into capillaries. The capillaries run from the nerve fiber layer to the outer plexiform layer. The choroidal layer is also rich in blood vessels. The chorio-capillaries supply blood to the RPE. The three nerve cell layers of retina thus have two distinct sources of blood supply depending on their location. The outer layer of rods and cones are supplied by the choroidal blood vessels while the inner ganglion cells and bipolar cells receive the retinal blood supply.

Optic disc and optic nerve

The signals generated by the photoreceptors are carried to the brain by the optic nerve. The nerve fibers originating from the ganglion cells join together, to form the optic nerve. The optic nerve exits the eye through the optic disc. The optic disc lies 3 mm nasal and 4 mm medial to the fovea.

Sclera

The sclera is the outer layer of the eye. It is relatively avascular and almost entirely collagenous. It provides continuous protection to the intraocular tissues. The collagenous structure and vasculature make the sclera a tough layer.

Optics of the eye

     The cornea and the lens together refract the light from a distant object onto the retina. The cornea has a fixed curvature and thus a fixed refractive power. But the image of near objects is formed behind the retina. In order to focus on the near objects, the lens with the help of the ciliary muscles changes its shape or 'accommodates' to focus the light on the retina forming a sharp image, Fig. 3. Thus accommodation by the lens allows the eye to adjust the vision to view a nearby object. The refracted light falls on the inner nerve fiber layer of retina, reaches the outer layer to activate the photoreceptor cells namely rods and cones. When activated, these photoreceptors send a signal which is transmitted to the brain through the optic nerve. The optical power of the lens is measured in Diopters. A Diopter (D) is the reciprocal of the focal length of the lens. The optical power of the normal human eye lens is 60D which corresponds to a focal length of about 16 mm.

Fig. 3. Accommodation.

http://hyperphysics.phy-astr.gsu.edu
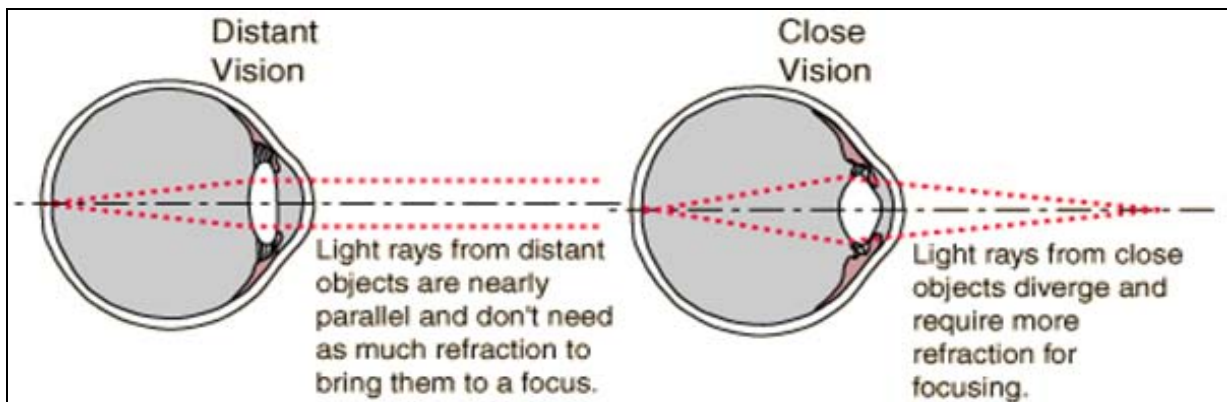
3. Ocular anomalies

Myopia

The lens focuses the incoming light onto the retina. It changes its shape to ensure that the focus is always on the retina. However in cases with an eye that is elongated, the distance between the lens and the retina increases, Fig. 4. The lens is now unable to focus the light on the retina as the retina has moved farther away. The focal point falls in front of the retina. The normal vision is thus affected and a person can see only a blurred image of a distant object. However a near object is seen clearly as its image now falls on the retina without the need of accommodation. Hence myopia is also called nearsightedness.
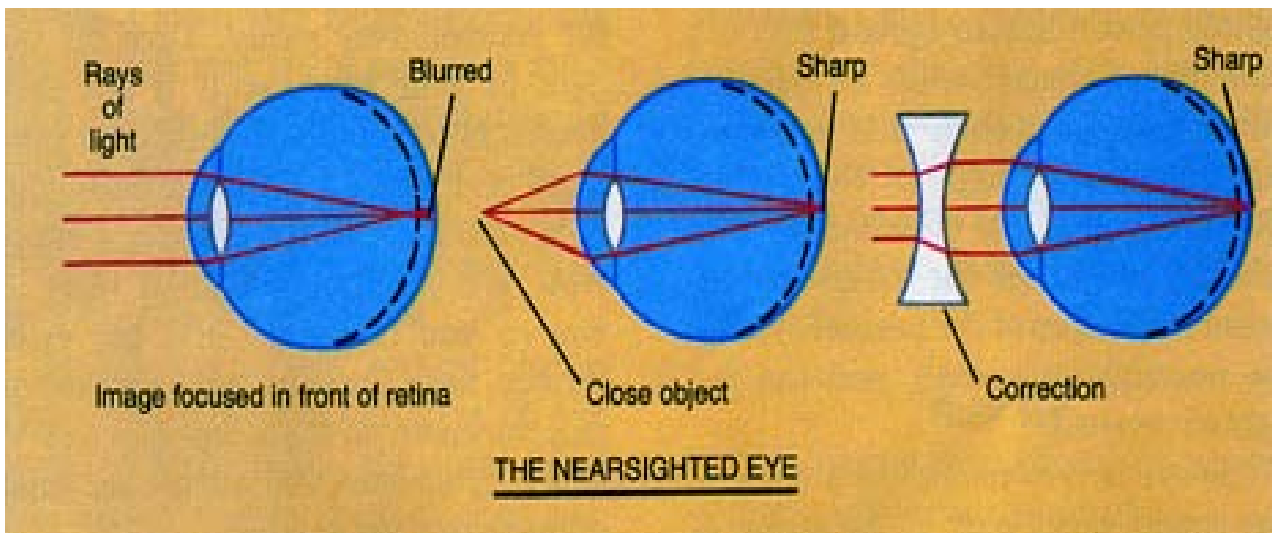
Fig. 4. Myopic eye.
www.medical-health.info/wp-content/uploads/20

The power of the corrective lens used to treat myopia helps in classifying myopia. Concave lenses are used to treat myopia as they help to focus the image farther from the eye. Myopia is classified as low myopia (corrective lens of power up to -3D), medium (-3 to -8D) and high myopia (corrective lens of the power above -8D). The refractive powers of the lens are additive. The power of the corrective lens when added to the crystalline lens of the eye will proportionately change the focal length so that the refracted light will fall on the retina. This is how optometrists prescribe lenses for myopic vision.

Retinal stretch in accommodation

The ciliary muscles help in accommodation as they change the shape of the lens in order to view objects at different distances. When the object is close to the eye, the ciliary muscles contract thereby releasing some of the pre-stress in the zonules making the lens more round. This process focuses the incoming light on to the retina. As a product of this process, the retina is stretched. Enoch[19] studied the effect of accommodation on retinal stretch and photoreceptor orientation using a monocular bisection test technique. His study suggests that 10 Diopters of accommodation stretched the retina by 2.4%. The angle subtended by an object on the retina at the lens is termed as visual angle. Accommodation induced retinal stretch increases the visual angle. Hollins [20] measured a retinal stretch of 4.5% between the ONH and the fovea as against a 2% stretch in the peripheral region of the retina using a fixation study. To view near objects, a myopic eye with corrective lenses would need to accommodate to see a sharp image. Thus the retina of a myopic eye would be stretched due to myopia as well as accommodation.

Retinal detachment

In old age the vitreous humor can shrink and detach from the retina. Myopic eye is at a higher risk of such retinal detachments. In myopia, the eye elongates to elliptical shaped globe. This structural change increases the traction exerted by the vitreous humor on the retina [21]. The vitreous humor begins to shrink and can detach from the retina. In either case, the vitreous humor exerts an increased centripetal traction force on the retina. The increased force and vitreous detachment can cause the retina to break. This type of retinal detachment causes photopsia or perceived flashes of light and floaters or deposits of RPE cells and blood inside the vitreous. Inflammation and severe acute hypertension sometime lead to accumulation of fluid in the sub-retinal space. The retina separates from the retinal pigment epithelium. RPE is the only channel of blood supply to the photoreceptors in the retina. When retina detaches from RPE, photoreceptors loose their metabolic and vascular support resulting in loss of vision.

Posterior staphyloma

In high myopia, the posterior pole of the eye is frequently observed to be protruding. This lesion is termed a posterior Staphyloma. In this disorder, the scleral shell is less stiff than

in the normal eye and expands gradually as well as it tends to thin out[22, 23]. The development of posterior Staphyloma may be due to excessive stretching of the posterior pole of the eye. It could lead to further complications such as myopic lesions [24], chorio-retinal atrophy and choroidal neo-vascularization. Angiographic studies showed choroidal neovascularizations to occur at the border of posterior Staphyloma in highly myopic eyes[25]. A Staphyloma that included the macular region was classified as Type II Staphyloma, Fig.5, and the depth of the Staphyloma is measured above the horizontal yellow line representing the plane of the optic disc in a B-scan ultra-sonographic image, Fig.6.
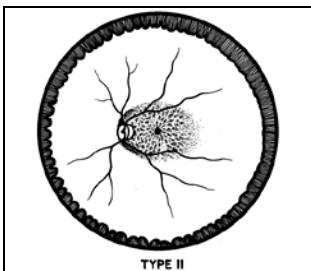
Fig. 5. Posterior staphyloma[23].
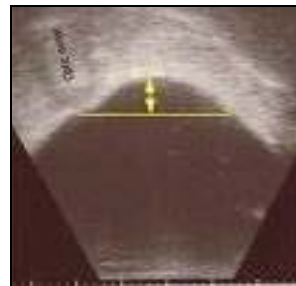
Fig. 6. B-scan ultra-sonographic image of posterior staphyloma. [24, 25]

Myopic crescent

The opening for the optic nerve in the retina and the choroid coincide in the normal eye. In Myopic eye, during elongation of the eye, the sclera is stretched, displacing the optic nerve opening towards the posterior pole. The optic nerve enters the scleral canal obliquely. The choroid and the retina terminate short before the optic disc on the temporal side. This leaves a bare sclera near the optic disc and is seen as a myopic crescent, Fig.7.[26]
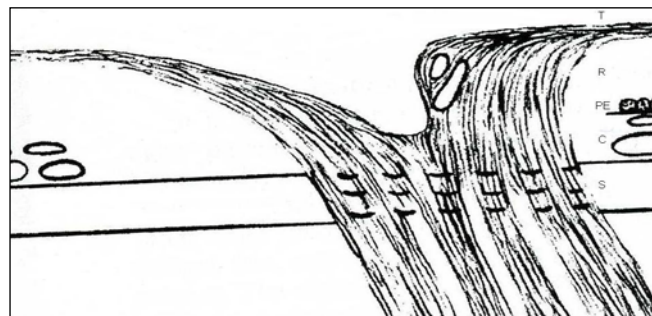
Fig.7. Myopic crescent. [26]
T-Temporal, R-Retina, PE-Pigment Epithelium,
C-Choroid, S- Sclera.

18

Macular degeneration (MD)

Age related MD

Degenerative changes in the macular region result in loss of useful central high acuity vision. Due to aging, tiny yellow or white accumulations of dead retinal cells, extra-cellular material build up between the RPE layer and choroid. These accumulations are termed 'Drusen'. Formation of drusen leads to dry macular degeneration. In further advancement of the disease, new blood vessels develop underneath the retina. The new blood vessels are leaky and cause accumulation of blood. This forms a dark spot in the central region of the frame that an eye is viewing. This type of macular degeneration is termed 'wet' MD.

Myopic macular degeneration

When myopia progresses, the axial length increases, stretching the retinal layers. The retina stretches in an attempt to conform to the elongated scleral shell. This additional stress can cause the chorio-capillaries to rupture leading to sub-retinal hemorrhage. The vision becomes blurred. The sub-retinal hemorrhage is a precursor for formation of lacquer cracks[27-29]. Sub-retinal hemorrhage also causes retinal detachment from Bruch's membrane. Choroidal Neovascularization (CNV) where in, the chorio-capillaries grow into the region of RPE through Bruch's membrane occurs[2]. These new vessels leak blood into the sub-retinal region.

Lacquer cracks

Lacquer cracks (LC) occur in 4.3% of high myopic eyes[30]. In a study by Curtin *et al*[22] of myopic macular degeneration the posterior pole exhibited cracks along with posterior staphyloma in 39.1% of eyes. These cracks maybe branched, criss-crossed or intricately distributed. They resemble the cracked lacquer on old wooden surfaces and hence are termed lacquer cracks. Stretching of the retina and choroid in staphyloma during myopia is seen as a major causative agent for crack formation[30]. These cracks appear at sites of sub-retinal hemorrhage in absence of CNV. Lacquer cracks represent mechanical breaks in the RPE and Bruch's membrane. CNV is observed subsequently. Hirata *et al*[31] studied micrographs of the regions of Bruch's membranes in the region of LC. They found that the delicate collagen fibrils

had ruptured and deeper collagen fibers were observed to orient diagonal or perpendicular to LC, Fig.8.
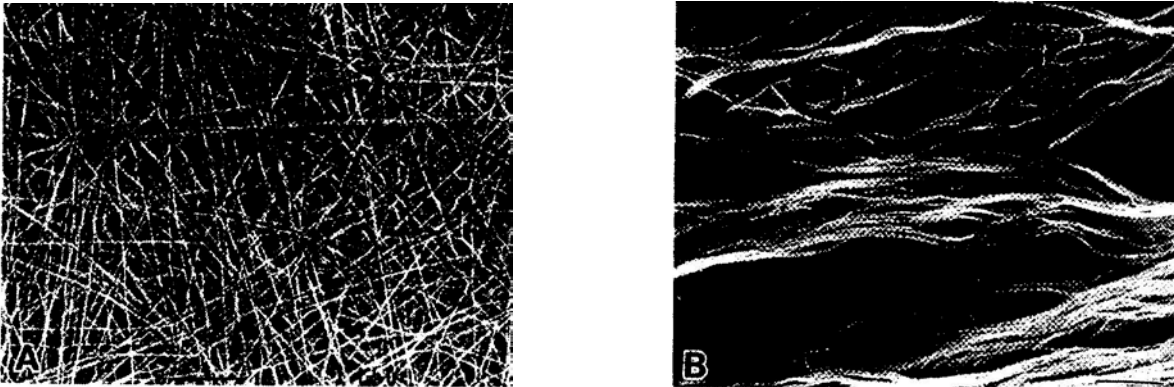
Fig.8. Rupture of collagen fibrils due to lacquer cracks.
8a. At a region away from the lesion (crack), collagenous fibrils form a delicate network .b. The network of collagenous fibrils at the site of the lesion is completely ruptured. The underlying thicker collagenous fibers are recognizable.[31]

In United States approximately 2% of the population is affected by pathologic myopia while in Asians the prevalence is 9%[24]. 2% of all myopes show myopic macular degeneration. Myopic macular degeneration is said to be the seventh greatest cause of blindness of adults in Europe and the USA, and has become the leading cause of blindness in Taiwan. (http://www.agingeye.net/myopia/1.7.php). Approximately 10% of patients 66 to 74 years of age will have findings of macular degeneration.

4. Detection and treatment of macular degeneration

Amsler grid

The Amsler Grid Test is one of the simplest and most effective methods for patients to monitor the health of the macula. The Amsler Grid is, in essence, a pattern of intersecting lines (identical to graph paper) with a black dot in the middle, Fig. 9a. The central black dot is used for fixation (a place for the eye to stare at). With normal vision, all lines surrounding the black dot will look straight and evenly spaced with no missing or odd looking areas when fixating on the grid's central black dot. When there is disease affecting the macula, as in macular degeneration, the lines can look bent, distorted and/or missing, Fig. 9b.
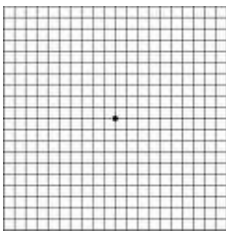
Fig.9a.Amsler grid
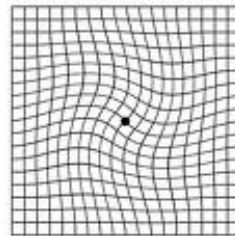
Fig.9b. Amsler grid as seen by
an eye affected with MD.

Angiography

To evaluate the extent of the damage from macular degeneration, an ophthalmologist may use fluorescein angiography. In this procedure, fluorescein dye is injected into a vein in the arm and photographs are taken of the back of the eye as the dye passes through blood vessels in the retina and choroid, Fig.10. The doctor then uses these photographs to detect changes in macular pigmentation or to identify small macular blood vessels. The doctor may also suggest a similar procedure called indocyanine green angiography. Instead of fluorescein, a dye called indocyanine green is used. This test provides information that complements the findings obtained through fluorescein angiography.

Fig.10.Angiogram of left eye.
www.seebetterflorida.com/

Fig.11. Optical coherence tomography
http://www.bascompalmer.org/site/current/images/researchbio

Optical coherence tomography (OCT)

This non-invasive imaging test helps identify and display areas of retinal thickening or thinning, Fig.11. Such changes are associated with macular degeneration. This test can also reveal the presence of abnormal fluid in and under the retina or the RPE. It is often used to help monitor the response of the retina to macular degeneration treatments.
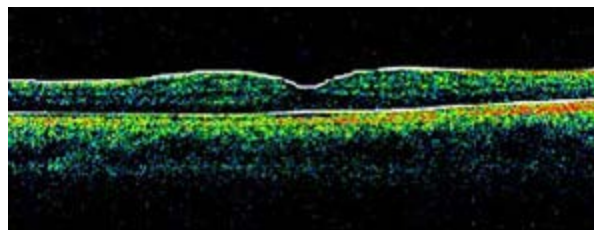
Treatment

Blindness in macular degeneration does not mean 'inability to see light' and even with far advanced macular degeneration the peripheral retina allows for useful vision. Lucentis (approved by US Food and Drug Association, FDA in June 2006) is the only drug that has been shown to improve vision in the settings of a controlled clinical trial. Lucentis (ranibizumab) is a humanized anti-VEGF (Vascular Endothelial Growth Factor) antibody fragment that inhibits VEGF activity by competitively binding with VEGF. The results from Lucentis clinical trials support its use to prevent further vision loss from wet macular degeneration. About one-third patients (34%-40%) gain vision after 12 months of treatment with Lucentis. All other available treatment options (Photocoagulation, PDT, Vitrectomy or Macugen) at best delay the inevitable vision loss but do not prevent ongoing vision loss. Macugen, approved by FDA in 2004, is a selective VEGF antagonist. It prevents growth of abnormal blood vessels and leakage of fluid and blood in retina. Photocoagulation is an effective treatment for extra-foveal CNV. It provides a short term benefit by reducing immediate vision loss. Disadvantages include scarring of retina and failure to prevent long term severe vision loss. Photodynamic therapy (PDT) is a painless procedure wherein a photosensitive drug is injected intravenously in to the patient's arm. A laser light activates this drug in the patient's eye. This treatment slows retinal damage but does not restore or prevent vision loss. Vitrectomy is a surgical extraction procedure. The rationale for this treatment is that relocating the fovea to an area where the retinal pigment epithelium is less diseased may allow for recovery of some useful vision.

5. Scope of research

Lacquer cracks are formed mainly due to mechanical factors in the myopic eye[16]. The macular region being considerably thinner (0.25 mm) and avascular than the peripheral retina, is highly susceptible to myopic elongation. The progression of myopia can be correlated to the stress in the retinal layer. This study aims to find the critical values of the stresses and related parameters involved in the progression of macular degeneration. These critical values will help predict the current stage of progression of MD. Finite Element method was used to model the myopic eye. Axis symmetric and 3D models of the posterior myopic eye were developed. These models included the retina, sclera, choroid and the optic disc. The effect of increasing intraocular pressure was studied in each model. Regions of high radial and compressive stresses were noted to predict failure locations of the myopic eye. Experimentation includes the study of material properties of Bovine Choroid using tensile and membrane test. Elastic modulus was calculated based on bending and stretching analysis of the results.

6. Mechanical engineering theories

A critical step in the lacquer crack formation is the stretching of retina due to elongation of the scleral shell. The mechanical factors involved in this process will determine the progress of degeneration and hence need to be evaluated. Evaluation of pressure, axial length and material properties may help to predict the onset and extent of macular degeneration. Various mechanical engineering theories, enlisted below, have been applied to the myopic eye to study the stresses induced.

A mechanical principle that has been applied to the eye and retinal stress calculation is Laplace's law. This is a stress formula that allows computation of stress on the walls of a thin pressurized spherical shell, Fig.12, as follows;

$$\sigma = \frac{Pr}{2t} \tag{1}$$

where σ is the biaxial stress, P is internal pressure, t is wall thickness and r is the radius of curvature.
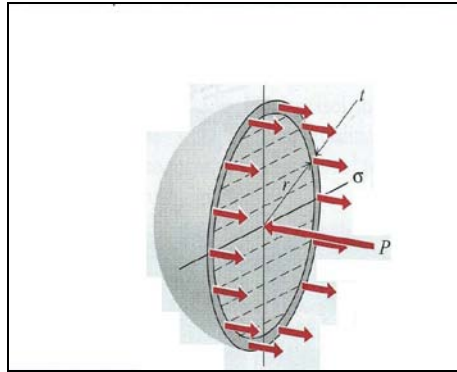
Fig. 12. Laplace's law.

Friedman[3] was the first to apply this formula to the eye, and many have used it since, even though the eye is not a complete sphere. Using this formula, it can be seen that due to the larger radius of curvature and reduced shell thickness, the highly myopic eye is theoretically exposed to higher levels of biaxial stress, Fig. 13. However, Perkins[6] after measuring the axial lengths, intraocular pressure and scleral thickness of emmetropic (normal) and myopic eyes was unable to detect any increase in stress within the highly myopic eye.

Fig.13.Biaxial stress.

Laplace's law fails to account for the effects of elasticity, which according to balloon studies[7],[32], alters the pressure and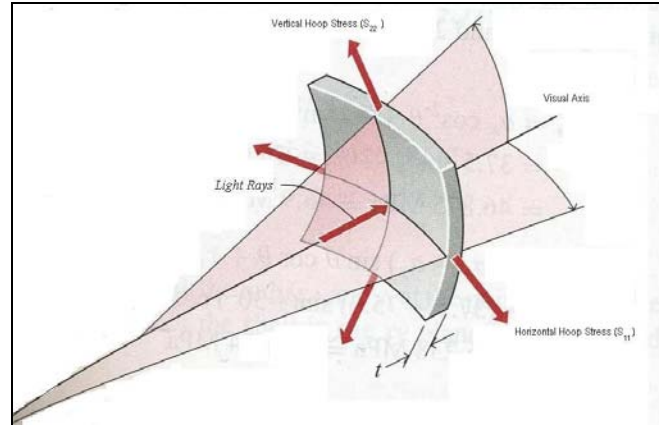 stress relationships. As the radius of the balloon increases, the radial resistance to stretch diminishes to a critical level, as there is a sudden expansion of the balloon. It is doubtful that the inflation characteristics of balloons can be applied directly to the elasticity of the retina. However, the balloon expansion phenomenon does call into question the usage of Laplace's law in estimates of wall stress within the retina.

Hole in a plate theory

Greene[4] has applied mechanical engineering principles to the problem of the myopic crescent, comparing the crescent to a porthole or a circular hole in a plate under tension. Similarly, this theory can be used to study the stress in the retina around the fovea.The stresses at the hole ($r = a$) for uniaxial tension are given to be, Fig.14a,

$$\sigma_{rr} = 0$$
$$\sigma_{\theta\theta} = T - 2T\cos(2\theta)$$
$$\sigma_{r\theta} = 0$$
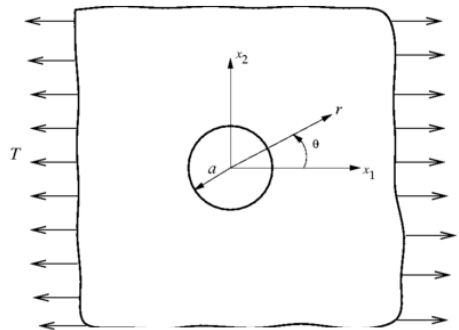
Fig.14a. Hole in plate under uniaxial stress.

The maximum hoop stress ($\sigma_{\theta\theta}$) will be at $\theta = 0$ or $\theta = \pi / 2$.

At $\theta = 0$, $\sigma_{\theta\theta} = -T$ (compressive)

At $\theta = \pi / 2$, $\sigma_{\theta\theta} = 3T$ (tension)

For biaxial stress, using principle of superposition at $\theta = 0$ and $\theta = \pi / 2$, Fig.14b,

$$\sigma_{\theta\theta} = 3T + (-T) = 2T \tag{2}$$

Fig.14b. Hole in plate under biaxial stress.

Buckling of thin plates

The flexural rigidity (D) of a thin circular plate is given by,

$$D = \frac{Eh^3}{12(1-v^2)} \tag{3}$$

where E is modulus of elasticity, h is thickness, v is Poisson's ratio.
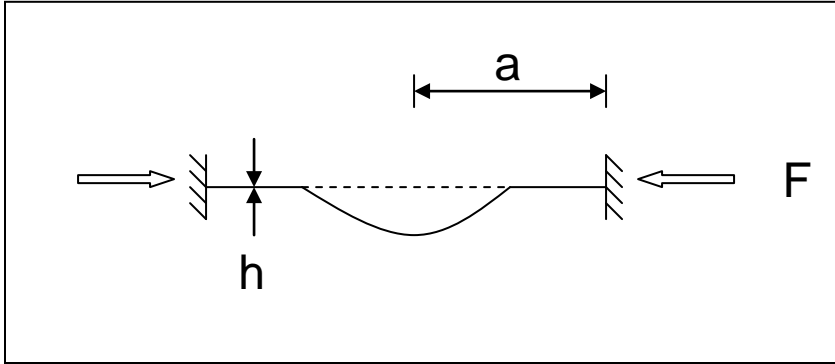
Fig. 15. Buckling of plate.

The critical value of the compressive stress (σ_{rr}) for buckling of a circular thin plate with clamped edges[33], Fig. 15,
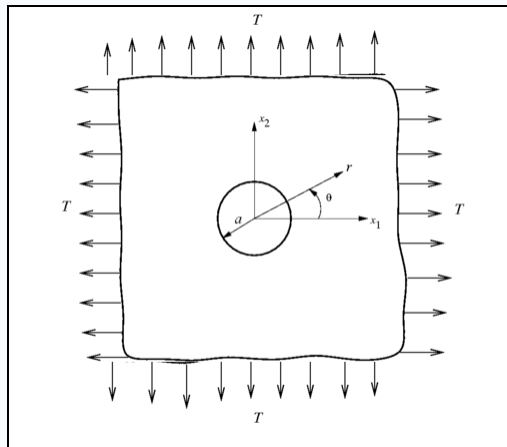
$$\sigma_{rr} = -\frac{14.7D}{a^2 h} \tag{4}$$

and from (4), we can write the critical value of compressive stress for the plate to buckle,

$$\sigma_{rr} = -\frac{14.7Eh^2}{12(1-v^2)a^2} \tag{5}$$

where a is radius of plate, 14.7 is equal to the square of the smallest root of $J_1(\alpha a)$; the Bessel function part of the general solution for the differential equation of the deflection surface of the plate[33].

This theory might be useful to study the fovea if it was considered to be a thin circular plate subjected to radial compression due to the intraocular pressure (IOP). It would be worthwhile to investigate whether the increased radial stresses due to myopia were sufficient for the fovea to buckle and form a wrinkle.

7. Material properties

The retina was considered to be isotropic [34] and the modulus of elasticity for the retina of different animals has been calculated experimentally. Wollensak *et al* [35]estimated the modulus of porcine retina using a simple tension test in air to be around 100 kPa. They also tested the choroid similarly to determine its elastic modulus as 1 MPa. Jones *et al* [36]graded the force required to pull the retina. Then mathematically modeled the deformed profile and a value of 10 kPa calculated for the Young's modulus of the bovine eye. Friberg *et al* [37]performed tensile tests on choroid and sclera to estimate values of moduli as 200 to 800kPa for the choroid and 3 MPa for the sclera. Phillips *et al* [38]estimated the scleral modulus as 2.5MPa for induced myopic Tree shrew eyes. Woo *et al* [39]estimated the scleral modulus of human eyes to be 5.5MPa where as Sigal *et al* [10]have used a modulus of 3MPa for their FEA of ONH. Biomaterials such as the retina, behave as hyper-elastic Mooney –Rivlin materials. Mooney-Rivlin constants for primate retina[9] suggest that the ratio of modulus of elasticity of the fovea to the vascularized area around it is about 1:10. This indicated that the Young's modulus for the fovea was 10 times less than that used for the rest of the retina.

Study of non-linear material

The material properties of the retina closely resembled that of a Mooney-Rivlin hyper-elastic material [9, 40] for vulcanized rubber.

U (I_1, I_3, I_3) is the strain energy function, where principal invariants are function of principal stretches (λ),

$$I_1 = \lambda_1^2 + \lambda_2^2 + \lambda_3^2$$

$$I_2 = \lambda_1^2\lambda_2^2 + \lambda_2^2\lambda_3^2 + \lambda_3^2\lambda_1^2 \qquad (6)$$

$$I_3 = \lambda_1^2\lambda_2^2\lambda_3^2$$

Subject to the regularity assumption that U is continuously differentiable infinitely many times with respect to I_1, I_2, I_3, we may write U (I_1, I_3, I_3) as an infinite series[41],

$$U(I_1, I_2, I_3) = \sum_{p,q,r=0}^{\infty} c_{pqr} (I_1 - 3)^p (I_2 - 3)^q (I_3 - 1)^r \tag{7}$$

The form of the Mooney-Rivlin strain energy potential is[42]

$$U = c_{10}(I_1 - 3) + c_{01}(I_2 - 3) + \frac{1}{D_1}\left(J^{el} - 1\right)^2 \tag{8}$$

where J^{el} is the elastic volume ratio, D_1 is a constant which is inversely proportional to initial bulk modulus (K_0). Also J is the total volume ratio which is the ratio of volume to original volume, J^{th} is the thermal volume ratio, ε is the normal strain, ε^{th} is the thermal strain.

$$J^{el} = \frac{J}{J^{th}}, J = (1 + \varepsilon)^3 = \frac{V}{V_o}, J^{th} = (1 + \varepsilon^{th})^3$$

$$K_0 = \frac{2}{D_1}$$

Incompressible materials

For an incompressible material $I_3 = 1$, $J^{el}=1$ and U depends on only two independent deformation invariants[41],

$$U(I_1, I_2) = \sum_{p,q=0}^{\infty} c_{pq} (I_1 - 3)^p (I_2 - 3)^q \tag{9}$$

with $c_{00} = 0$. From (7) with $I_3 = 1$, we get

$$I_1^2 \geq 3I_2 \qquad\qquad I_2^2 \geq 3I_1 \tag{10}$$

Mooney-Rivlin strain energy function for incompressible material is given by,

$$U(I_1, I_2) = c_{10}(I_1 - 3) + c_{01}(I_2 - 3) \tag{11}$$

For an incompressible material,

$$\lambda_1 \lambda_2 \lambda_3 = 1$$

The stress is given as,

$$\sigma_1 = \frac{\partial U}{\partial \lambda_1} = c_{10} \frac{\partial}{\partial \lambda_1} (\lambda_1^2 + \lambda_2^2 + \frac{1}{\lambda_1^2 \lambda_2^2} - 3) + c_{01} \frac{\partial}{\partial \lambda_1} (\lambda_1^2 \lambda_2^2 + \frac{1}{\lambda_1^2} + \frac{1}{\lambda_2^2} - 3)$$

$$\sigma_1 = 2c_{10}(\lambda_1 + \lambda_2 \frac{\partial \lambda_2}{\partial \lambda_1} - \frac{1}{\lambda_1^3 \lambda_2^2} - \frac{1}{\lambda_1^2 \lambda_2^3} \frac{\partial \lambda_2}{\partial \lambda_1}) + 2c_{01}(\lambda_1 \lambda_2^2 + \lambda_1^2 \lambda_2 \frac{\partial \lambda_2}{\partial \lambda_1} - \frac{1}{\lambda_1^3} - \frac{1}{\lambda_2^3} \frac{\partial \lambda_2}{\partial \lambda_1})$$

For an uniaxial stress,

$$\lambda_2 = \lambda_3 = \frac{1}{\sqrt{\lambda_1}}$$

$$\sigma_1 = 2c_{10}(\lambda_1 + \lambda_1^{-\frac{1}{2}} \frac{\partial \lambda_1^{-\frac{1}{2}}}{\partial \lambda_1} - \frac{1}{\lambda_1^3 \lambda_1^{-1}} - \frac{1}{\lambda_1^2 \lambda_1^{-\frac{3}{2}}} \frac{\partial \lambda_1^{-\frac{1}{2}}}{\partial \lambda_1}) + 2c_{01}(\lambda_1 \lambda_1^{-1} + \lambda_1^2 \lambda_1^{-\frac{1}{2}} \frac{\partial \lambda_1^{-\frac{1}{2}}}{\partial \lambda_1} - \frac{1}{\lambda_1^3} - \frac{1}{\lambda_1^{-\frac{3}{2}}} \frac{\partial \lambda_1^{-\frac{1}{2}}}{\partial \lambda_1})$$

$$\sigma_1 = 2c_{10}(\lambda_1 - \frac{1}{2} \lambda_1^{-2} - \frac{1}{\lambda_1^2} + \frac{1}{2} \lambda_1^{-2}) + 2c_{01}(1 - \frac{1}{2} - \frac{1}{\lambda_1^3} + \frac{1}{2})$$

$$\sigma_i = 2(c_{10} + \frac{c_{01}}{\lambda_i})(\lambda_i - \frac{1}{\lambda_i^2})$$

$$(12)$$

Substituting for stretch in (12), we get for small strain

$$\sigma = 2\left(c_{10} + \frac{c_{01}}{1+\varepsilon}\right)\left(1+\varepsilon - \frac{1}{(1+\varepsilon)^2}\right)$$

$$\sigma = 2\left(c_{10} + \frac{c_{01}}{1+\varepsilon}\right)\left(1+\varepsilon - \frac{1}{(1+2\varepsilon+\varepsilon^2)}\right)$$

$$\sigma \cong 2(c_{10} + c_{01}(1-\varepsilon))(1+\varepsilon - 1 + 2\varepsilon)$$

$$\sigma = 6(c_{10} + c_{01})\varepsilon$$

$$(13)$$

which gives the modulus of elasticity for Mooney-Rivlin material as,

$$E = 6(c_{10} + c_{01}) \tag{14}$$

For an incompressible material in equi-biaxial stress,

$$\lambda_1 \lambda_2 \lambda_3 = 1$$

The Mooney Rivlin equation for biaxial stress condition can be derived as,

$$\sigma_1 = \frac{\partial U}{\partial \lambda_1} = \frac{\partial}{\partial \lambda_1}\left[c_{10}\left(\lambda_1^2 + \lambda_2^2 + \frac{1}{\lambda_1^2 \lambda_2^2} - 3 \right) + c_{01}\left(\frac{1}{\lambda_1^2} + \frac{1}{\lambda_2^2} + \lambda_1^2 \lambda_2^2 - 3 \right) \right]$$

$$\sigma_1 = \left[2c_{10}\left(\lambda_1 + \lambda_2 \frac{\partial \lambda_2}{\partial \lambda_1} - \frac{1}{\lambda_1^3 \lambda_2^2} - \frac{1}{\lambda_1^2 \lambda_2^3}\frac{\partial \lambda_2}{\partial \lambda_1} \right) + 2c_{01}\left(-\frac{1}{\lambda_1^3} - \frac{1}{\lambda_2^3}\frac{\partial \lambda_2}{\partial \lambda_1} + \lambda_1 \lambda_2^2 + \lambda_1^2 \lambda_2 \frac{\partial \lambda_2}{\partial \lambda_1} \right) \right]$$

For a biaxial stress,

$$\lambda_1 = \lambda_2 = \lambda_3^{-\frac{1}{2}}$$

$$\sigma_1 = \left[2c_{10}\left(2\lambda_1 - \frac{2}{\lambda_1^5} \right) + 2c_{01}\left(\frac{-2}{\lambda_1^3} + 2\lambda_1^3 \right) \right]$$

$$\sigma_i = 4\left(c_{10} + c_{01}\lambda_i^2 \right)\left(\lambda_i - \frac{1}{\lambda_i^5} \right)$$

(15)

Behavior of Mooney-Rivlin material

The uniaxial stress plot, Fig.16, showed softening effect where as the equi-biaxial stresses, Fig. 17, initially showed softening up to 20% strain and then had material hardening. Also, the effect of varying the ratio of the Mooney-Rivlin constants was plotted in both these figures.
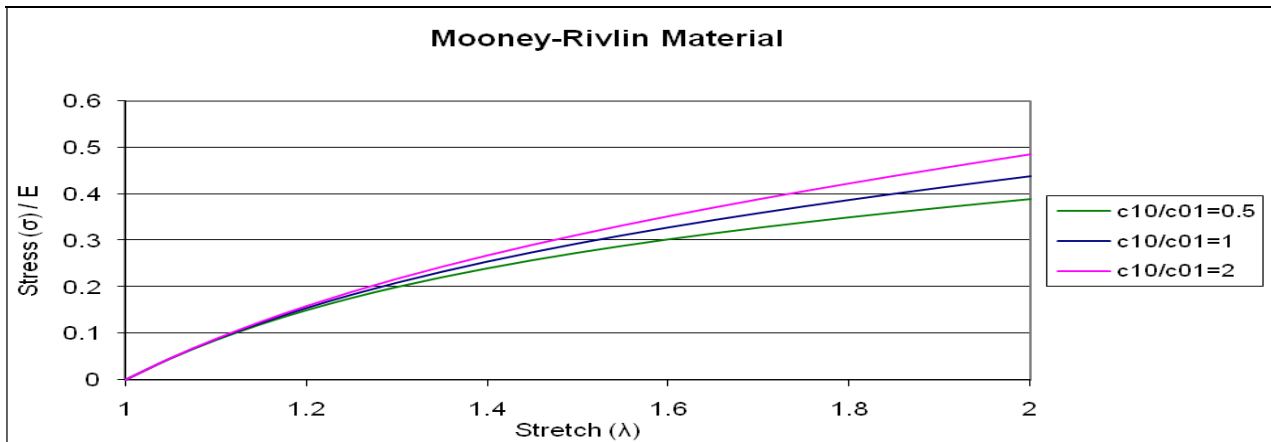

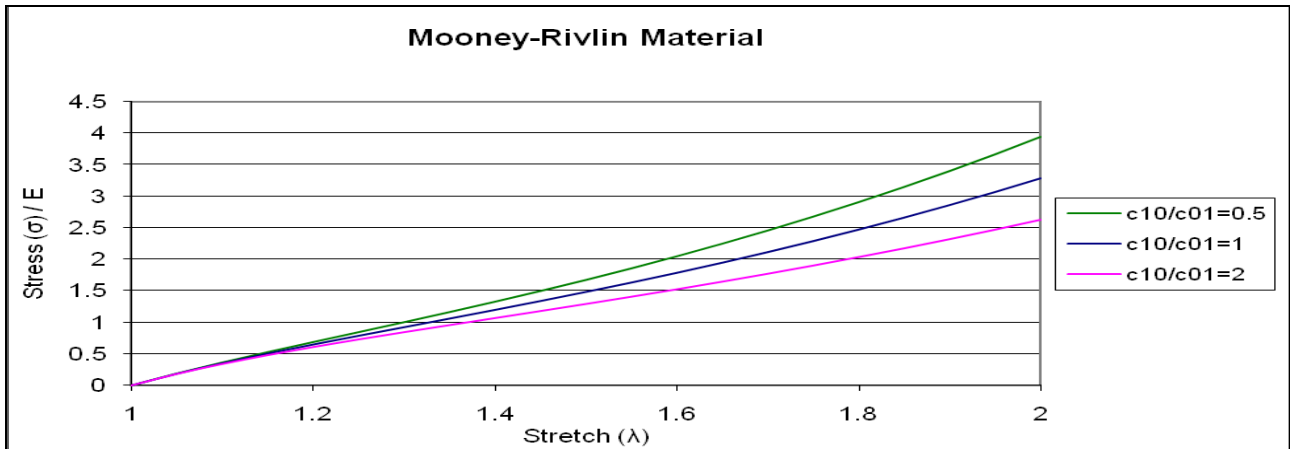Fig. 16. Variation of Mooney-Rivlin constants in uniaxial stress.

Fig. 17. Variation of Mooney-Rivlin constants in biaxial stress.

A stress-strain relation for porcine eye was given by the tensile test data curve by Wollensak, Fig.18[35]. The retina was modeled to have a bilinear material behavior to fit the data of porcine eyes. The retina yielded at 8.3 kPa and had a breaking stress of 12kPa.
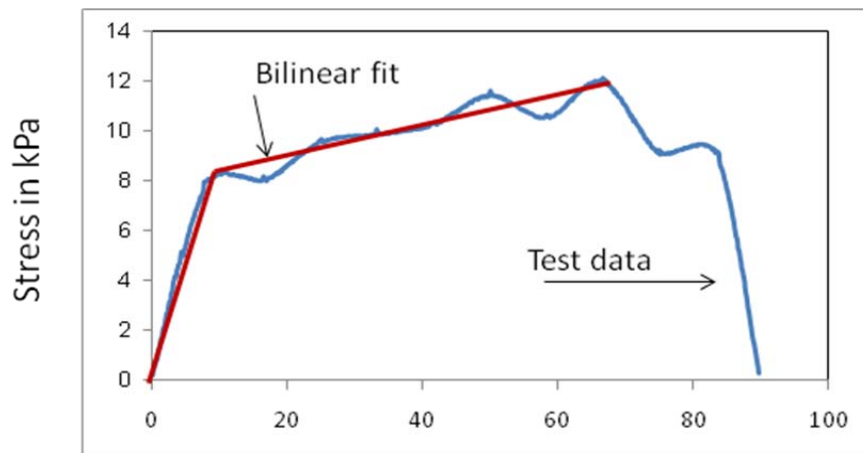

Fig.18.Experimental data for retina by Wollensak.

Based on the test data and using 'Evaluate' feature in Abaqus, Mooney-Rivlin constants were c_{10} = -11,765 Pa and c_{01} = 27,000 Pa. Calculated values of Mooney-Rivlin constants were used in (14) to get an approximate Young's modulus of 90kPa. The plot of Mooney-Rivlin material for uniaxial tensile loading showed a softening effect whereas the biaxial loading curve showed a linear behavior in the plotted stress range, Fig. 19.
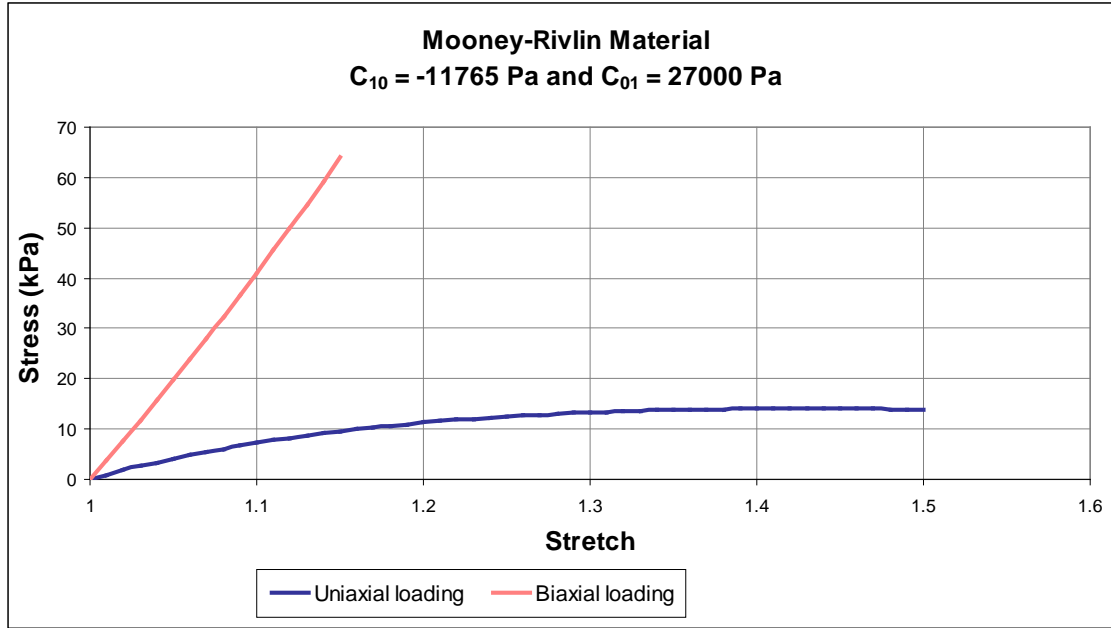
Fig.19. Mooney-Rivlin material with evaluated constants.

The comparison of all the material models (linear, bilinear, hyperelastic) used for the retina in Abaqus analysis is shown in Fig.20.
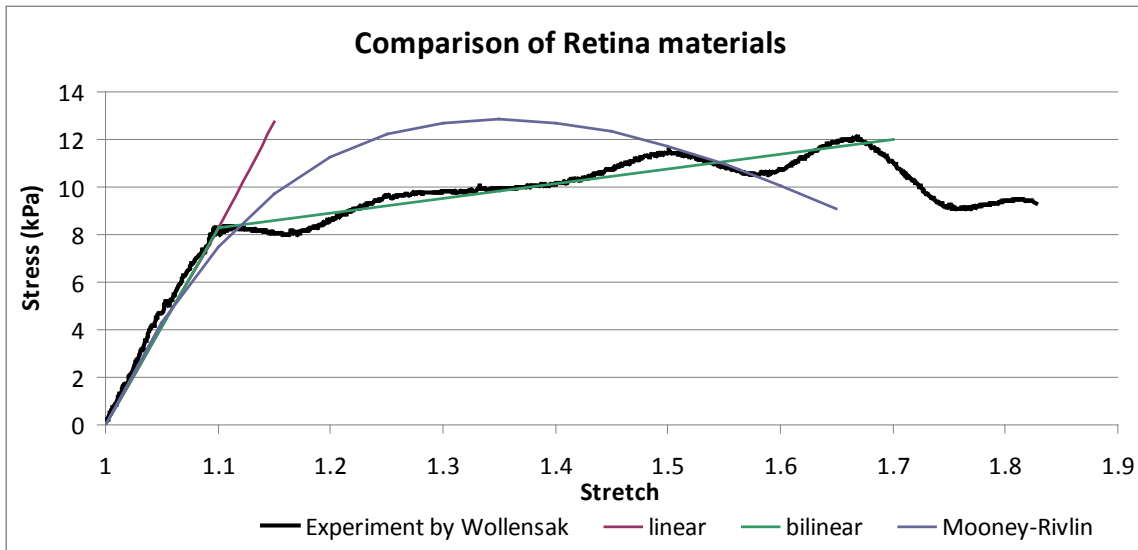

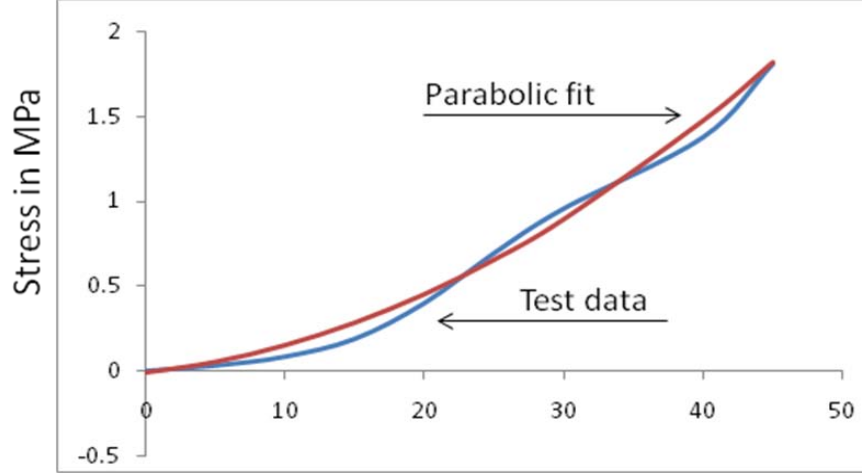Fig. 20. Comparison of retina material.

Fig. 21.Experimental data for choroid by Wollensak.

The choroid was modeled to have isotropic hyper-elastic material based on the test data of tensile testing previously done by Wollensak, Fig.21,[35]. The test data was fit using a parabola which when evaluated by Abaqus matched the Ogden strain energy potential (n=1) for μ=240kPa and α=12 approximately. The Ogden model is typically used for soft-tissue material with large deformation. Hu *et al*[43] have characterized soft tissue material for large deformations using Ogden and Mooney Rivlin model in their study. The optic disc was assigned linear elastic material with Young's modulus of 3MPa [12].

The strain energy function for an Ogden model (n=1) is given as,

$$U = \frac{2\mu}{\alpha^2}\left(\lambda_1^{\alpha} + \lambda_2^{\alpha} + \lambda_3^{\alpha} - 3\right)$$

where μ (shear modulus) and α are temperature dependant material properties.
For an incompressible material,

$$U = \frac{2\mu}{\alpha^2}\left(\lambda_1^{\alpha} + \lambda_2^{\alpha} + \frac{1}{\lambda_1^{\alpha}\lambda_2^{\alpha}} - 3\right) \tag{16}$$

For an uniaxial stress state,

$$\lambda_2 = \lambda_3 = \lambda_1^{-\frac{1}{2}}$$

$$\sigma_1 = \frac{\partial U}{\partial \lambda_1} = \frac{2\mu}{\alpha^2} \frac{\partial}{\partial \lambda_1}\left[\lambda_1^\alpha + 2\lambda_1^{-\left(\frac{\alpha}{2}\right)}\right]$$

$$\sigma_i = \frac{2\mu}{\alpha}\left[\lambda_i^{\alpha-1} - \lambda_i^{-\left(1+\frac{\alpha}{2}\right)}\right]$$

(17)

which can be simplified for small strain as,

$$\sigma = \frac{2\mu}{\alpha}\left[(1+\varepsilon)^{\alpha-1} - (1+\varepsilon)^{-\left(1+\frac{\alpha}{2}\right)}\right]$$

$$\sigma \cong \frac{2\mu}{\alpha}\left[1+(\alpha-1)\varepsilon - 1 + \left(1+\frac{\alpha}{2}\right)\varepsilon\right]$$

$$\sigma \cong 3\mu\varepsilon$$

(18)

Thus the modulus of elasticity can be approximated as,

$$E = 3\,\mu$$

(19)

For a biaxial stress state,

$$\lambda_1 = \lambda_2 = \lambda_3^{-\frac{1}{2}}$$

$$\sigma_1 = \frac{\partial U}{\partial \lambda_1} = \frac{2\mu}{\alpha^2} \frac{\partial}{\partial \lambda_1}\left(2\lambda_1^\alpha + \lambda_1^{-2\alpha} - 3\right)$$

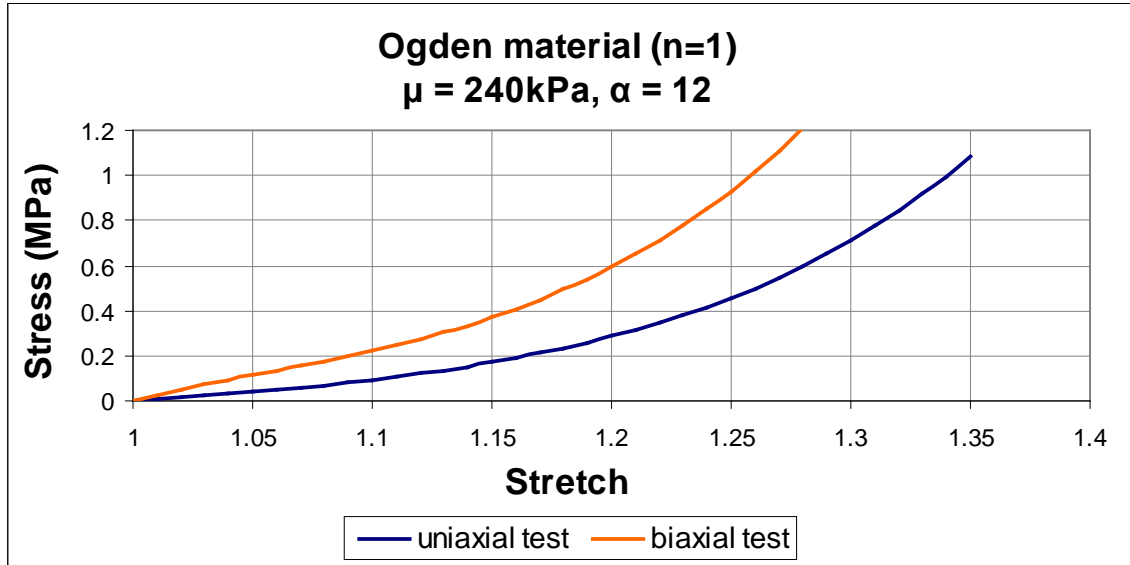$$\sigma_i = \frac{4\mu}{\alpha}\left[\lambda_i^{\alpha-1} - \lambda_i^{-(1+2\alpha)}\right]$$

(20)

Fig.22.Ogden material for evaluated constants.

The stress-stretch relation for Ogden material (n=1) with μ=240 kPa and α=12 for uniaxial and biaxial loading is shown, Fig.22. The Young's modulus for the choroid for small strain can be calculated as 720 kPa from (19). The effect of variation of α is shown in Fig.23a and Fig.23b.
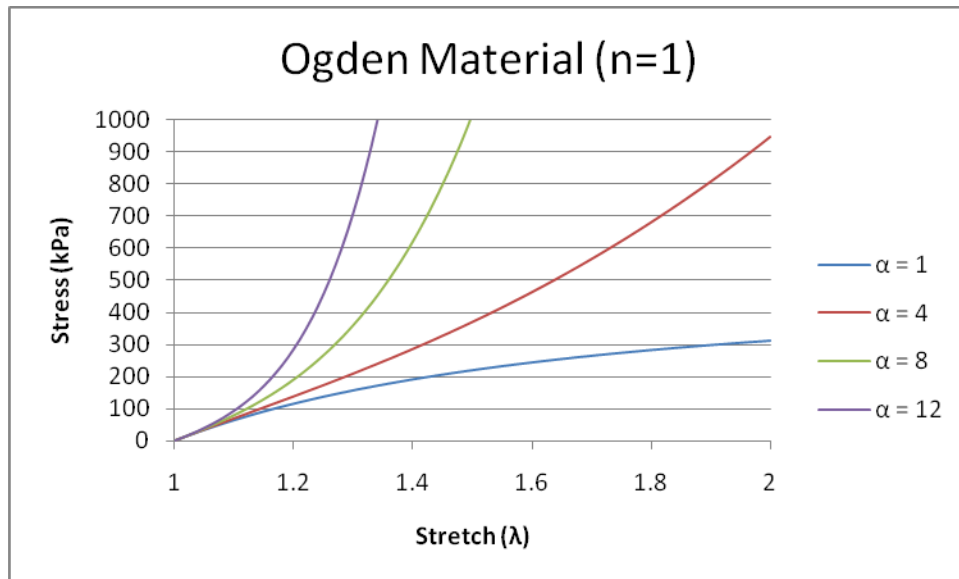

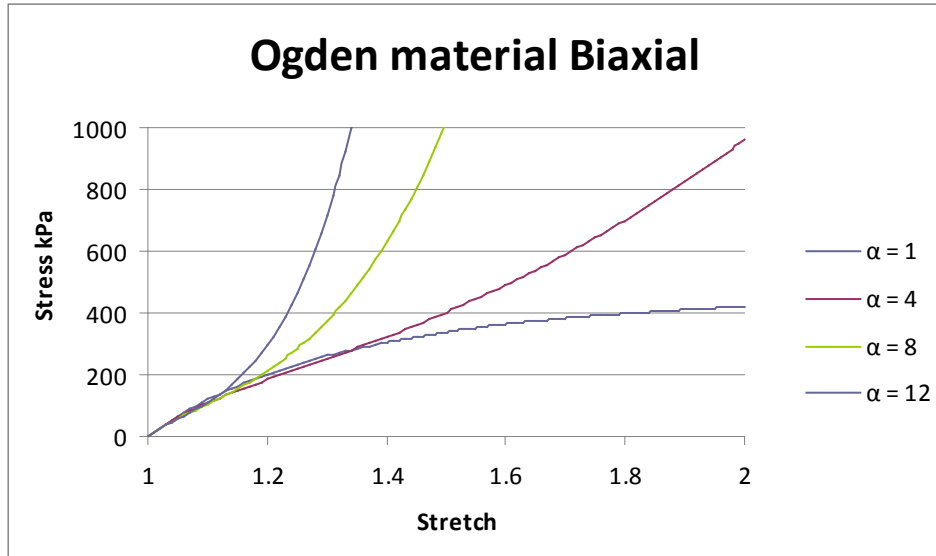Fig.23a. Variation of Ogden constant for uniaxial stress.

Fig.23b. Variation of Ogden constant for biaxial stress.

8. Finite element modeling

Model 1: Axisymmetric linear elastic no contact model

Finite Element Modeling was carried out in ABAQUS 6.7(Simulia, Providence, RI). The retina was modeled about the visual axis of symmetry to resemble a hemispherical shell, Fig. 24a. The radius of the eye was approximated as 10mm. The thickness of the retina was 400µm. The modeled retina part comprised of the nerve fibril layers up to the choroid. The retina had a Young's modulus of 83 kPa with a Poisson's ratio of 0.499[10] to model it as nearly incompressible. Eight-node biquadratic axisymmetric quadrilateral reduced integration (1542) elements were used for modeling. The center of the retina was constrained to displace axisymmetrically along the visual (Y) axis. The edge was connected with four springs to model its attachment at the ora serrata. A stiffness of 75 kN/m for each spring was used. The spring constant was calculated as one tenth that of the retina material. The normal intraocular pressure (IOP) is 15mmHg (2kPa) in human eye. The analysis was carried at 15mmHg, 20mmHg (2.666kPa) and 25mmHg (3.334kPa) to study the effect of increasing IOP on the retina.

Fig.24a.FE model-1.
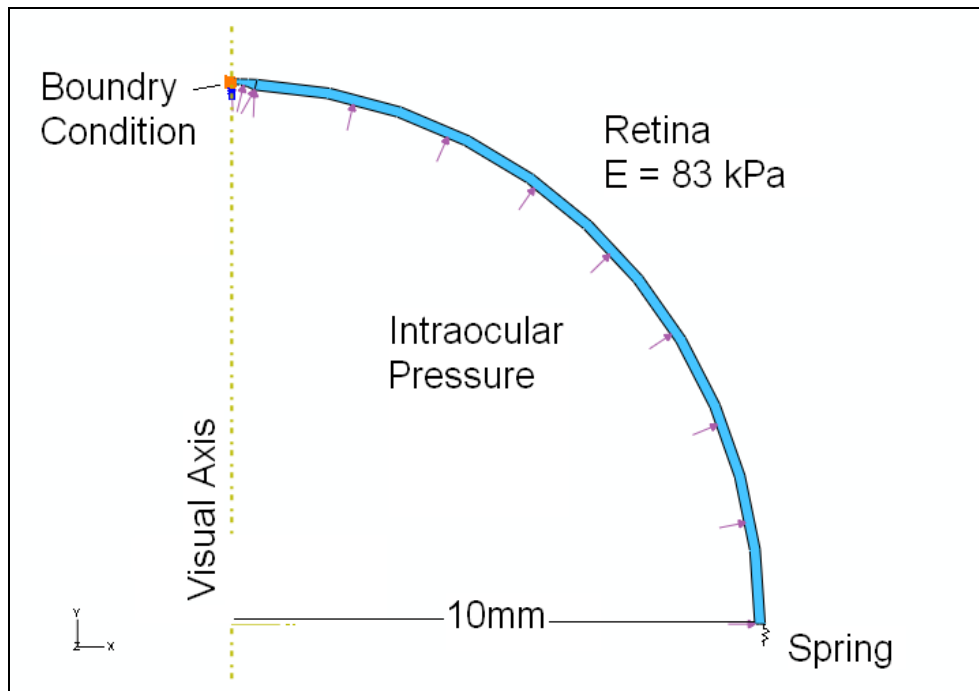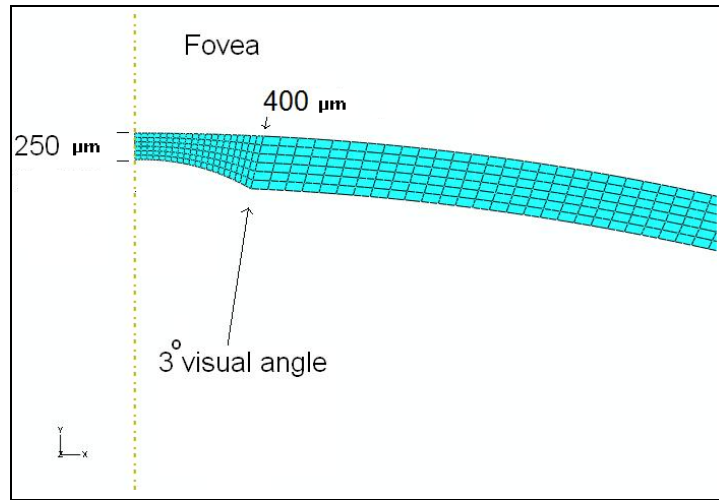
Fig.24b. Meshing of model-1.

The fovea had a denser mesh to study the stress in detail, Fig.24b. It was 500 μm in radius [9] which subtends an angle of about 3° from the center of the eye. The thickness of the fovea was 250 μm in the center and was gradually increased to 400 μm at its outer edge to match the retina. The fovea had a stiffness equal to that of the retina (E= 83 kPa) in model 1.

Model 2: Axisymmetric Mooney-Rivlin hyperelastic contact model

The sclera was incorporated along with the retina in model 2, Fig.25. It was a concentric ellipsoidal arc and had an eccentricity (e) along the visual axis (Y axis) of 1mm with respect to the retina. This mismatch would replicate the situation of the retina trying to conform to the elongated sclera in myopia. A Mooney-Rivlin hyperelastic material from Wollensak's(Fig.18) [35] tests with elastic modulus approximately 90kPa was used in model 2 with the fovea an order of magnitude less stiff than rest of the retina. The Mooney-Rivlin constants when calculated using the 'Evaluate' feature were c_{10}=-11.765kPa and c_{01}=27kPa. A static frictionless surface-to-surface contact was defined between the retina and the sclera. The sclera being more rigid than the retina was treated as the master surface. Eight-node biquadratic axis-symmetric quadrilateral reduced integration (1320) elements were used for modeling the retina and two-node axisymmetric linear rigid link type (112) elements for the sclera.
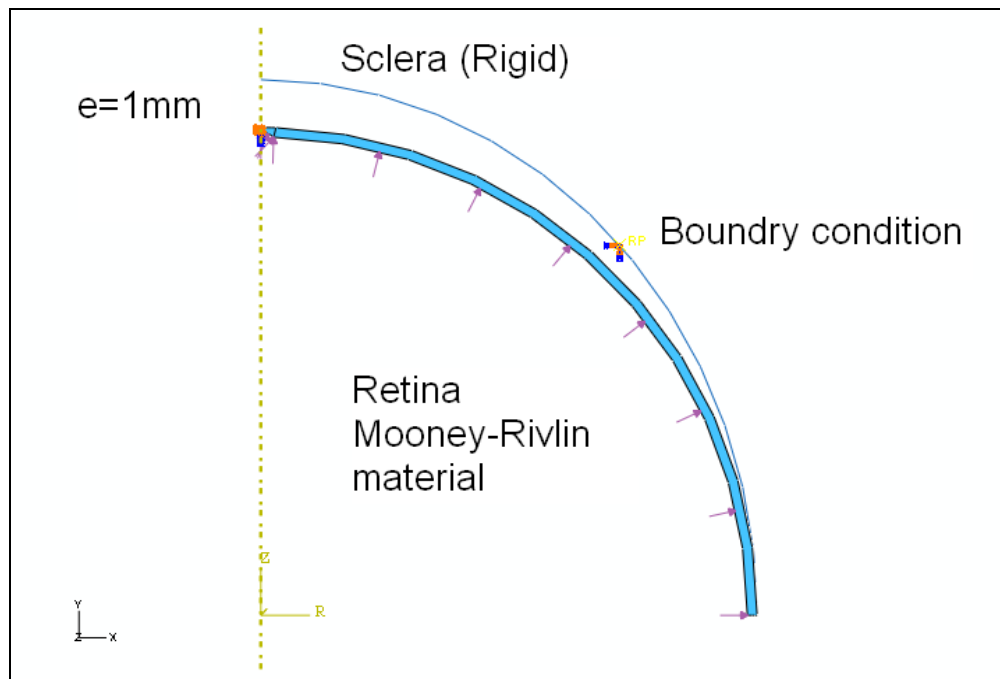

Fig. 25. FE model-2.

Model 3: Axisymmetric, contact, bilinear retina and parabolic choroid material
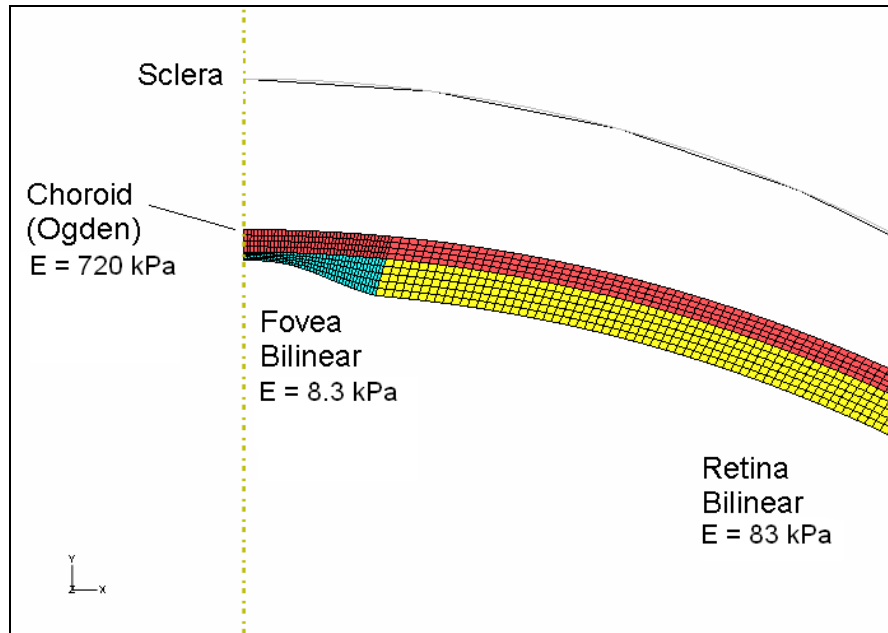

Fig. 26. FE model-3.

Model 3 incorporated a choroid layer on the outer side of the retina, Fig.26. The retina was modeled to have a bilinear material behavior based on the test data by Wollensak, Fig.18. The fovea is void of any vasculature and had material properties one order of magnitude less stiff as that of the retina with modulus of 8.3kPa. The choroid was stiffer than the retina due to the blood vessel network in it. The choroid material was defined by a parabolic stress-strain relation which was fitted by an Ogden strain energy potential (n=1) with μ=240kPa and α=12 using the 'Evaluate' feature in Abaqus. The value of μ represents a Young's modulus of 720kPa for the choroid according to (19). Soft tissues with Ogden strain energy potential (n=1) have been noted to have α=14[44] and α=12[43] previously. The value of α for the choroid as evaluated by Abaqus is comparable to those of soft tissues and thus accepted for model 3. The boundary conditions, contact interactions and loads were applied as in the case of model 2. Eight-node biquadratic axisymmetric quadrilateral reduced integration (2763) elements were used for modeling the retina and two-node axisymmetric linear rigid link type (100) elements for the sclera.

41

Model 4: Three dimensional, contact with bilinear retina, Ogden choroid and linear elastic optic disc
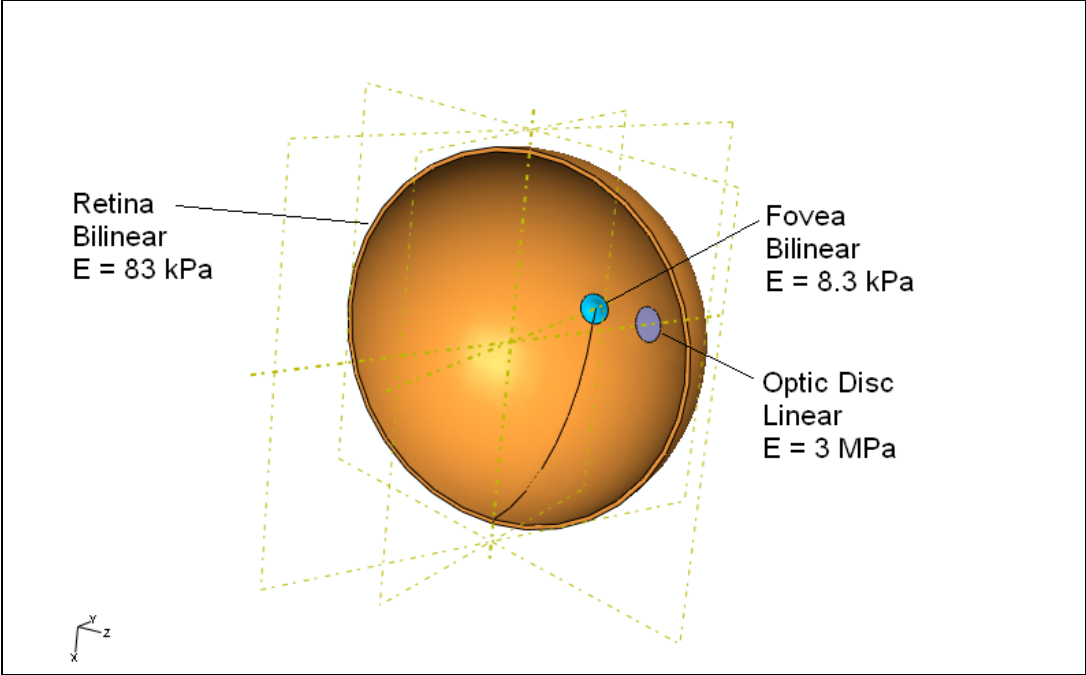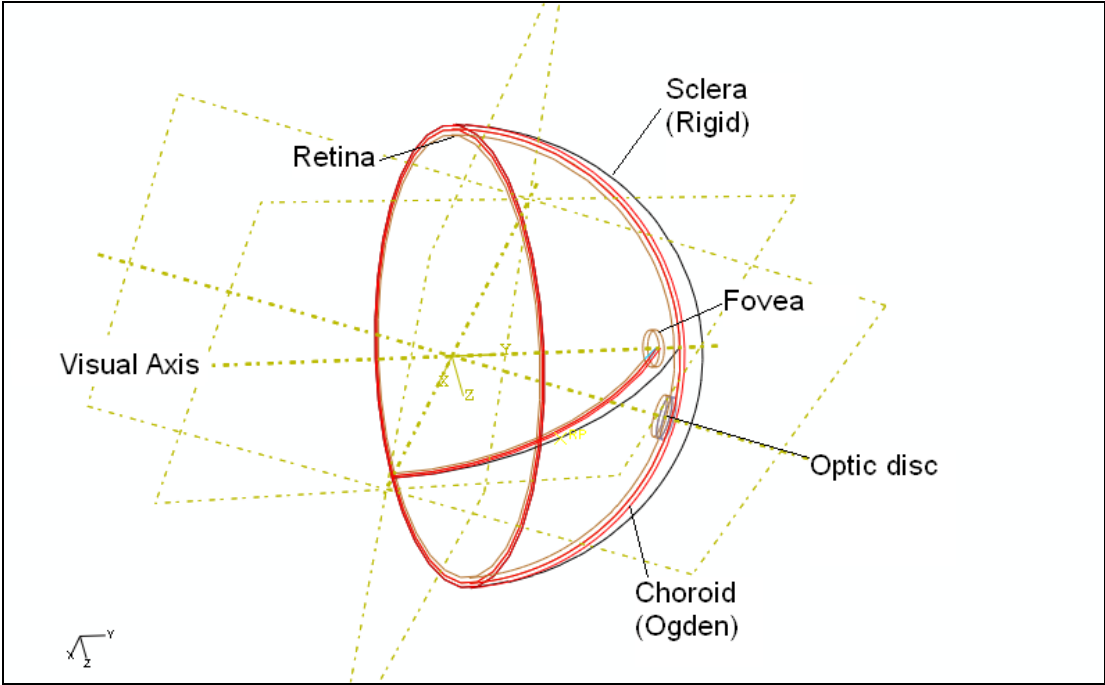

Fig. 27. FE model-4 retina.

Fig. 28. FE model-4 assembly.

A three dimensional model of the retina was developed in Abaqus. The model consisted of a layered hollow hemisphere representing the retina with a thinned fovea pit at the apex, Fig.27. The choroid was bonded on the external surface of the retina. The fovea was free of any vascularization and thus had modulus of 8.3kPa as in model 3. The sclera was concentric ellipsoid with an eccentricity of 1mm, Fig.28. The equatorial radius of the retina and sclera were 10mm as in previous models. The thickness of the retina was 250micron as the choroid was excluded in model 4. The thickness of the retina was reduced to 100 micron at the apex having a 1.74 mm diameter circular region representing the fovea (dimple). The optic disc with 1.5 mm in diameter was located 3 mm nasal and 4 mm medial to the fovea, Fig.28. The optic disc was relatively thrice stiffer as the choroid[12]. A frictionless surface contact was defined for the choroid with the sclera. The sclera was rigid and fixed in position. The retina and choroid were pinned at its edges. A regular ten-node tetrahedron reduced integration (47449) element mesh was generated for the retina and choroid part. The sclera was meshed using three-node 3-D triangular facet type (2328) elements. The model was loaded as in previous models.

9. Experimentation

Preparation of sample

Mechanical experimentation was performed on samples of young calf eyes (Research 87, Boylston, MA). Fresh Bovine eyes were dissected to separate the scleral shell from the rest of the eye. The eyes were stored at -80 degree Celsius for future use. The eyes were thawed to room temperature before experimentation. The vitreous humor was gently removed and the retina was cut at the optic nerve head. The retina was lifted away from the eye. The Choroid was gently peeled using a razor blade. The thickness of the choroid was measured using a micrometer to be approximately 300µm (h).

Experiment 1: **Membrane test**

A nano universal testing machine (Agilent Technologies, Santa Clara, CA) was used to measure the indenter force and fixture displacement. The indenter consisted of a cylindrical shaft with a hemispherical steel ball of 2 mm in diameter (2R), Fig.29a,b,. For membrane test, a 10mm (2a) O-ring was glued using PT-28 (Pacer Technologies, Rancho Cucamonga, CA) to the inner surface of the choroid, Fig.30. Care was taken to prevent any visible wrinkles/folds during adhesion of the O-ring. The choroid was placed on the fixture in a cavity filled with PBS saline solution (Phosphate Buffered Saline- 1X at room temperature). The concave surface of the choroid was placed facing the indenter. The fixture top plate having a central hole for the indenter was clamped to the base of the fixture. The fixture was moved towards the indenter to submerge the tip into the saline. The fixture was advanced towards the indenter at the rate of 1 mm/min up to approximately 5 times the thickness of the choroid. The sample was unloaded at the same rate as the loading. This measurement was repeated several times until the sample maintained its position and did not tear.
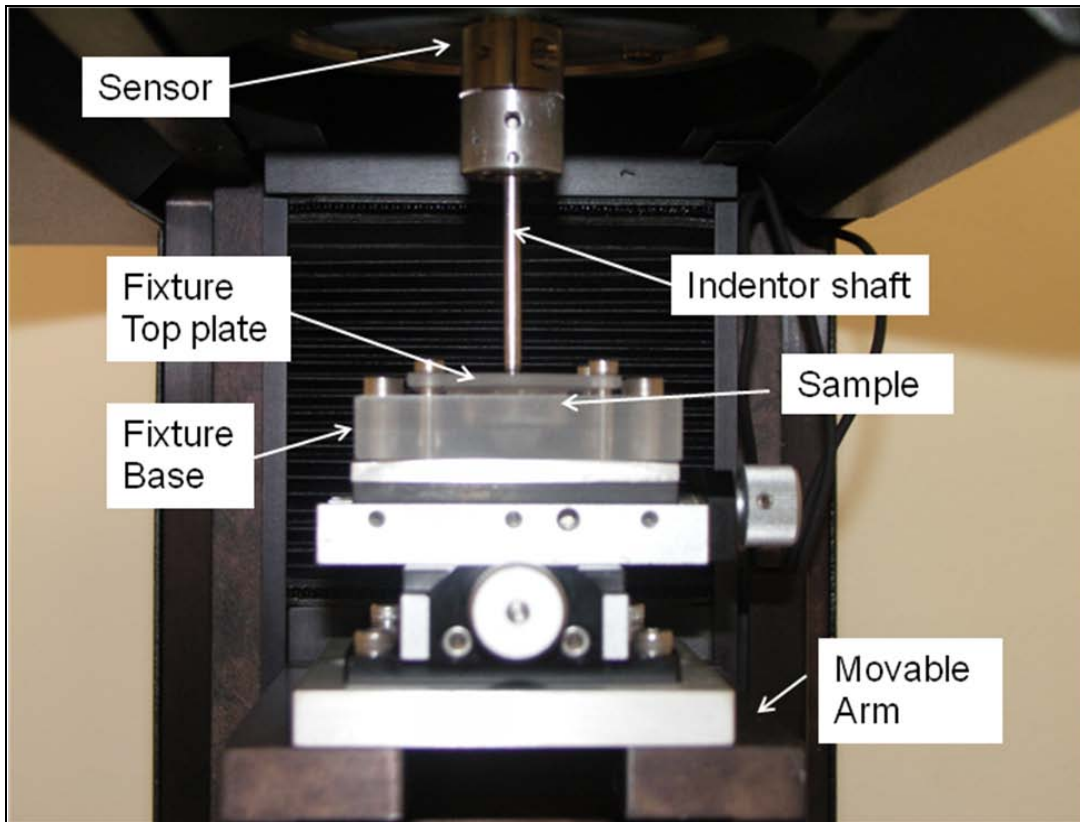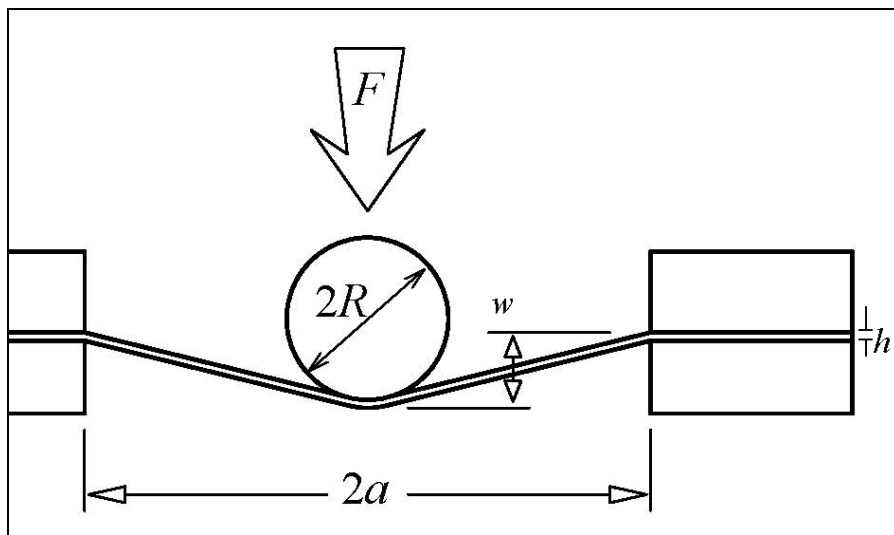
Fig. 29a. Experimental setup for membrane test.

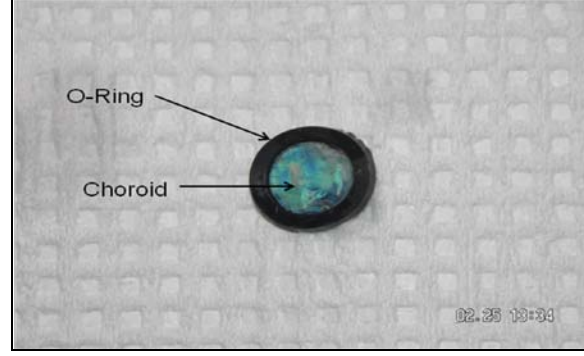Fig. 29b.Schematic for membrane test.

Fig. 30. Choroid sample.

The circular membrane was compared to a circular plate with center point load. The equation for bending analysis by Timoshenko[45] was used to estimate the modulus of elasticity of the material. Biomaterials are considered to be incompressible and a Poisson's ratio of 0.5 was used for calculation. To calculate the stretching caused during the test, we used the relation provided by Wan *et al*[46] for the membrane test with center point loading. The transition between bending to stretching was also analyzed using a numerical solution by Wan *et al.*[47]

$$w_{bending} = \frac{3a^2}{4\pi h^3}\left(\frac{1-v^2}{E}\right)F \tag{21}$$

$$w_{stretch} = \left(\frac{4a^2}{\pi h}\right)^{1/3}\left(\frac{1-v^2}{E}\right)^{1/3}F^{1/3} \tag{22}$$

$$W = \frac{\varphi}{\beta^2}\left\{\left[\frac{1-\beta K_1(\beta)}{\beta I_1(\beta)}\right][1-I_0(\beta)]-\log\left(\frac{2}{\beta}\right)+\gamma+K_0(\beta)\right\} \tag{23}$$

where
$$W = \frac{w}{h}$$
$$\varphi = \frac{Fa^2}{2\pi Dh} \quad , \quad D = \frac{Eh^3}{12(1-v^2)}$$

w is displacement, h is thickness of membrane, F is force, a is radius of membrane, $\gamma = 0.577216$ is the Euler-Mascheroni constant, β is the membrane stress and I_0, K_0, K_1 are Bessel functions, v is Poisson's ratio.

46

Experiment 2: **Tensile testing**

    After thawing the sample to room temperature, parallel strips of 5 mm width were cut from the central region of the choroid. These strips were placed on 100 micron thick cardboard with rectangular slots 10mm in length and 10mm in width. The strips were placed parallel to the rectangular slot's edges. The strips were glued using PT-01 and PT-22 (Pacer Technologies, Rancho Cucamonga, CA) to the cardboard avoiding any visible folding/ wrinkles. The choroid along with the glued cardboard was clamped to UTM machine's sensor on one end and the motored base on the other. The free vertical edges of the cardboard which were parallel to the choroid were cut off. The choroid was hydrated by adding 1 drop of PBS saline solution at the machine sensor end. Uni-axial tension tests were performed on the choroid sample at 10, 100 and 1000μm per second rate up to 3% strain, 10% strain and failure (sample breakage). The stress (σ) –strain (ε) relationship for uniaxial tensile test is given as,

$$\sigma = E\,\varepsilon \tag{23}$$

$$\sigma = \frac{F}{A}$$

$$\varepsilon = \frac{\delta}{L}$$

where E is modulus of elasticity, F is the force, A is cross section area, δ is change in length, L is original length of sample.

10. Results and discussion

For conventional engineering materials (metals) the Mises stress is generally applied to predict failure in multi-axial loading beyond the yield point. It is uncertain which stress measure is an indicator of failure for biological samples like the retina and choroid. Thus radial, circumferential as well as Mises stress distribution have been discussed along with their locations. Results for strain and deformation have been plotted and a possible correlation to the changes occurring in the eye has been provided.
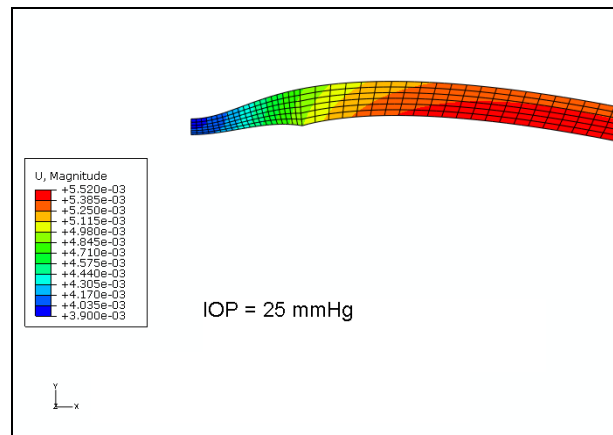
Model 1 : Results

Fig. 31.Model-1 deformation (U in meter).

The deformed shape of the retina showed radial expansion due to the applied intraocular pressure, Fig.31. The fovea moved towards the center of the retina. The deformation plot of the retina for 25 mmHg IOP had a magnitude of 5.52 mm. The deformation in the foveal region was 3.9 mm. This model does not include the sclera and thus the stress, strain and deformation were expected to be much greater than in reality. The Von Mises stress distribution for model 1 at 15 mmHg (2kPa) intraocular pressure (IOP) and 25 mmHg IOP were plotted, Fig.32a,b. The stress distribution in the fovea was studied in detail as this was the region of interest in studying macular degeneration. The Mises tensile stress varied from 2 kPa in the outer retina to 140 kPa in the inner retina for 15 mmHg IOP, Fig.32a. In the region away from the fovea, the Mises tensile stress was around 60kPa.
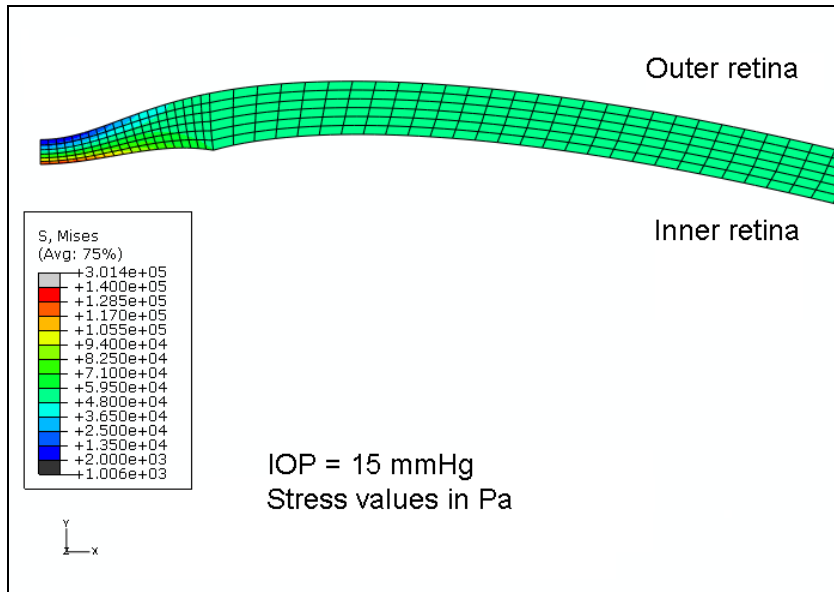
Fig. 32a. Mises stress distribution in model-1 for 15 mmHg.

The maximum Mises tensile stress increased as the pressure was increased. For 25mmHg, the maximum tensile Mises stress induced in the fovea was 220 kPa, Fig.32b. In the region away from the fovea, the Mises tensile stress was around 80kPa.
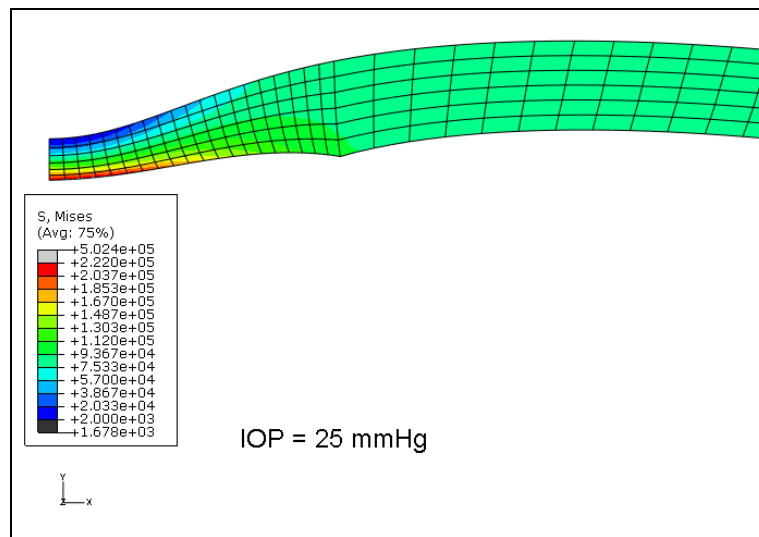

Fig. 32b. Mises stress distribution in model-1 for 25mmHg.
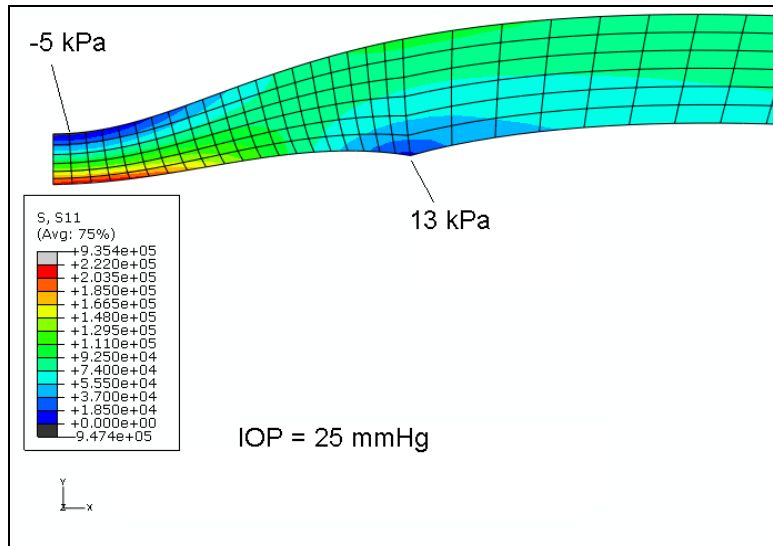
Fig. 33. Radial stress in model-1.

The plot of radial stress (S11) at 25mmHg showed a maximum tensile stress of 222 kPa on the inner side of the foveal region, Fig.33. A compressive radial stress of 5 kPa was observed on the outer edge of the fovea. A region of low tensile radial stress (13 kPa) was observed at the border of the fovea.

Fig. 34a. Radial strain in model-1.

The radial strain (E11) field in the fovea is shown for 25mmHg of IOP, Fig.34a. The maximum compressive radial strain had a magnitude of 0.45 and was located at the border of

the fovea on the inner retina, Fig.34a (left). The tensile radial strain was maximum in the inner retinal layer of the fovea at the center and had a 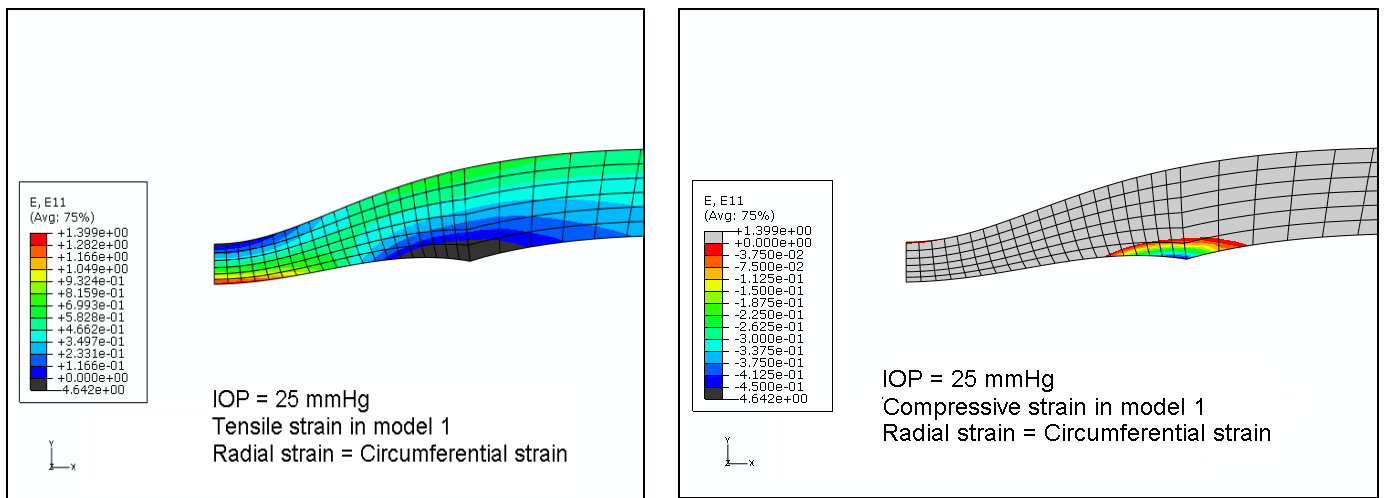magnitude of 1.399, Fig.34a(right). The circumferential stress (S33) and strain (E33) were nearly equal to the radial stress and strain values in the fovea.

Model 1 : Discussion

The circumferential and radial stresses in the fovea are comparable as the fovea lies at the symmetric axis. As radius of the location approaches zero the circumferential and radial stress become equal. The deformation of the outer region of the fovea towards the center was similar to the concept of foveal pit formation by Springer[9]. There was stress concentration at the edge of the fovea adjoining the retina due to surface discontinuity. The displacement of the retina was upto 5 mm which was half as compared to the radius of the eye. So model 2 onwards, the retina was modeled in the sclera to have more realistic values of deformation. Also the fovea region is avascular which is less stiff than the rest of the retina. The retina material was estimated to behave as a hyper-elatic Mooney-Rivlin model and thus the material used in model 1 needed modification. The wrinkling at the center of the fovea can be compared to the edges of an open ended cylinder with internal pressure, Fig.34b. The Mises and radial tensile stress were maximum on the inner central region of the fovea. A radial compressive stress was observed on the outer foveal region. The corner of the inner fovea with the retina had a stress concentration and needed smoothening around the curve. The results of model 1 indicated that the layers in the fovea were under maximum stress variation through the thickness than any other region of the retina. Model 1 suggested that the foveal region was under maximum stress and it was important to study the mechanics of this region in detail.
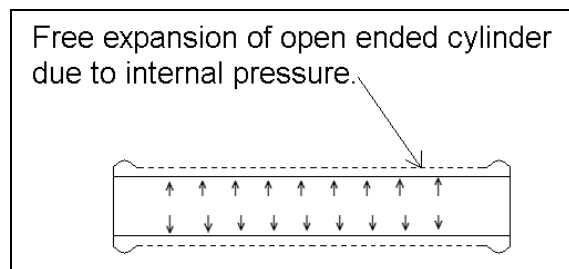

Fig.34b. Wrinkling of the edges of a cylinder.

Model 2 : Results

There was complete contact of the retina with the sclera at 15 mmHg. The maximum tensile Mises stress of 23.94 kPa was observed just outside the fovea for normal IOP of 15mmHg, Fig.35. The Mises stress in the fovea was in the range of 2 kPa to 5.7 kPa. The tensile Mises stress in the rest of the retina was between 10 kPa to 16 kPa.
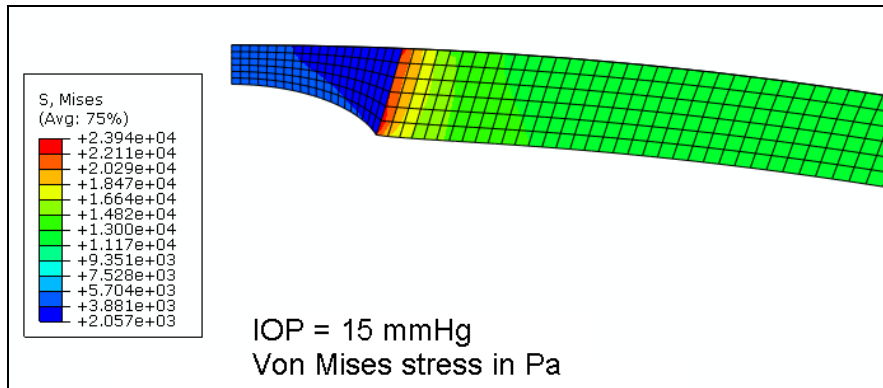

Fig. 35.Mises stress in model-2.
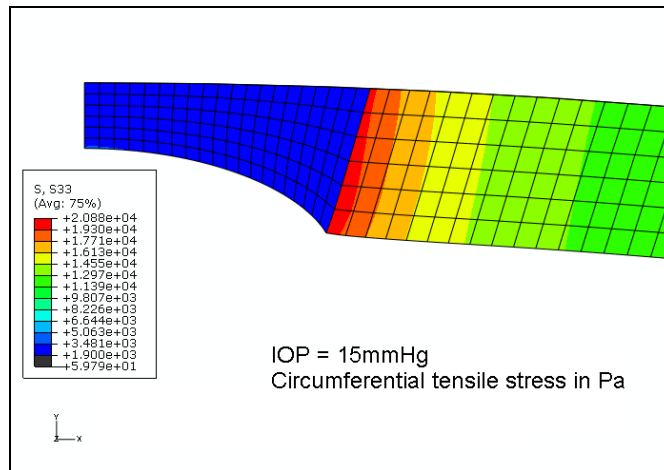
Fig. 36.Circumferential stress in model-2.

The circumferential tensile stress (S_{33}) distribution in model 2 for 15mmHg was qualitatively similar to the Mises stress, Fig.36. A maximum value of 20.88 kPa was observed just outside the fovea. The fovea had a range of circumferential tensile stress between 1.9 kPa to 3.48 kPa. The circumferential tensile stress in the retina outside the fovea ranged from 9.8 kPa to 19.3kPa. The radial tensile stress showed a region of reduced stress near the border of the fovea and the retina, Fig.37 (left). The radial stress was 3.5 kPa at the center of the fovea, reduced to 1 kPa near the border of the fovea and then increased in the retina. A small region

of radial compressive stress was observed at the corner of the fovea with maximum compressive stress of 1.3kPa, Fig. 37(right).

Fig.37. Radial stress in model-2 at 15 mmHg.

Fig.38. Strain in model-2 at 15 mmHg.

The circumferential strain, Fig.38(left) and the radial strain, Fig.38(right) were maximum at the fovea. The maximum strain was 0.30 in both directions and was located in the inner retinal region of the fovea. The maximum tensile Mises stress of 34.58 kPa was observed just outside the fovea for normal IOP of 25mmHg, Fig.39(left). The Mises stress in the fovea was in the range of 2.89 kPa to 10.82 kPa. The tensile Mises stress in the rest of the retina was between 16 kPa to 30 kPa. The circumferential tensile stress (S_{33}) distribution for 25mmHg was

qualitatively similar to the Mises stress, Fig.39(right). A maximum value of 29.34 kPa was observed just outside the fovea.
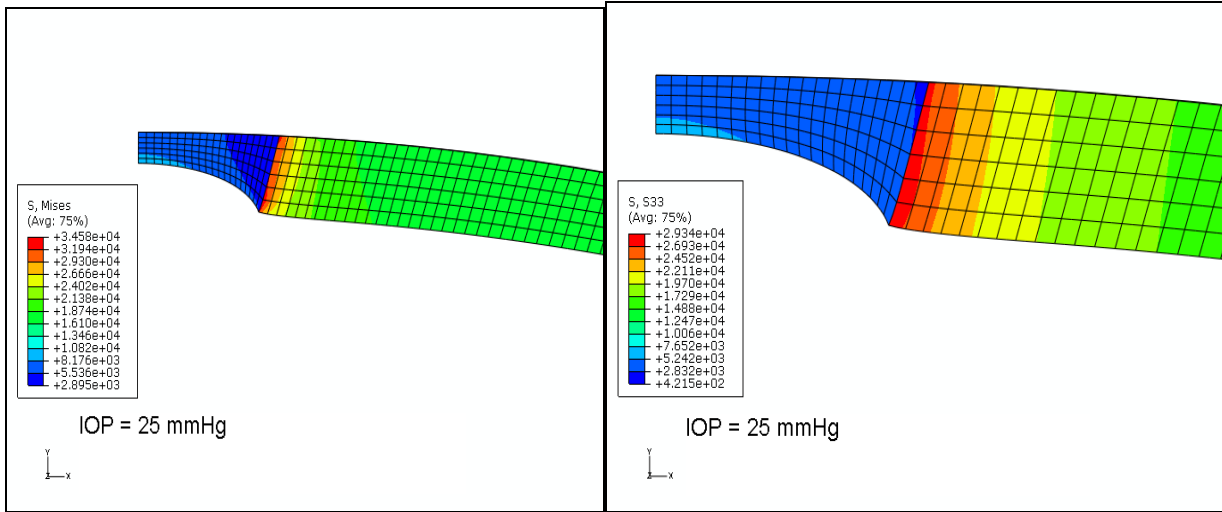
Fig.39. Mises (left) and circumferential stress (right).

Fig.40. Radial stress in model-2 at 25 mmHg.

The radial tensile stress showed a region of reduced stress near the border of the fovea and the retina, Fig.40 (left). The radial stress was 6 kPa at the center of the fovea, reduced to 1kPa near the border of the fovea and then increased in the retina. A small region of radial compressive stress was observed at the corner of the fovea with maximum compressive stress of -2.2 kPa, Fig. 40(right).
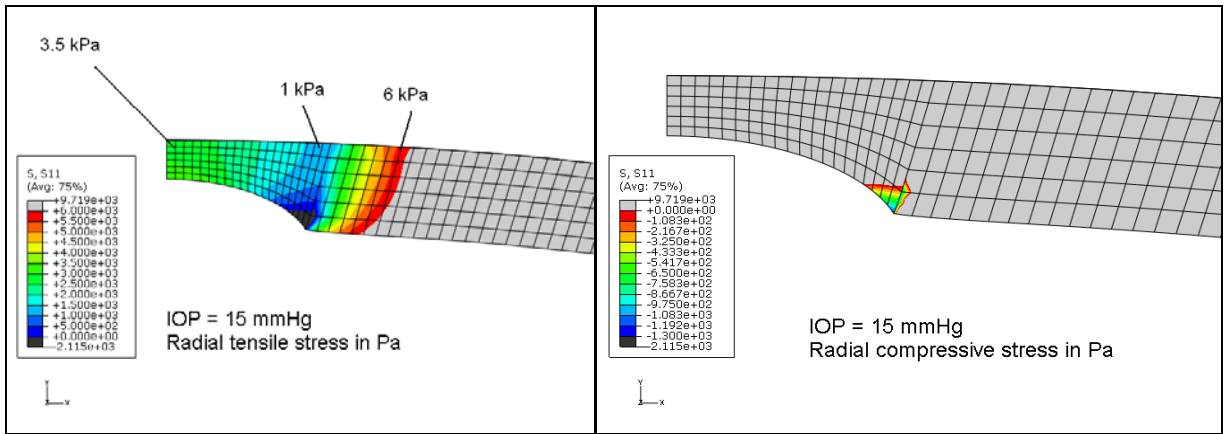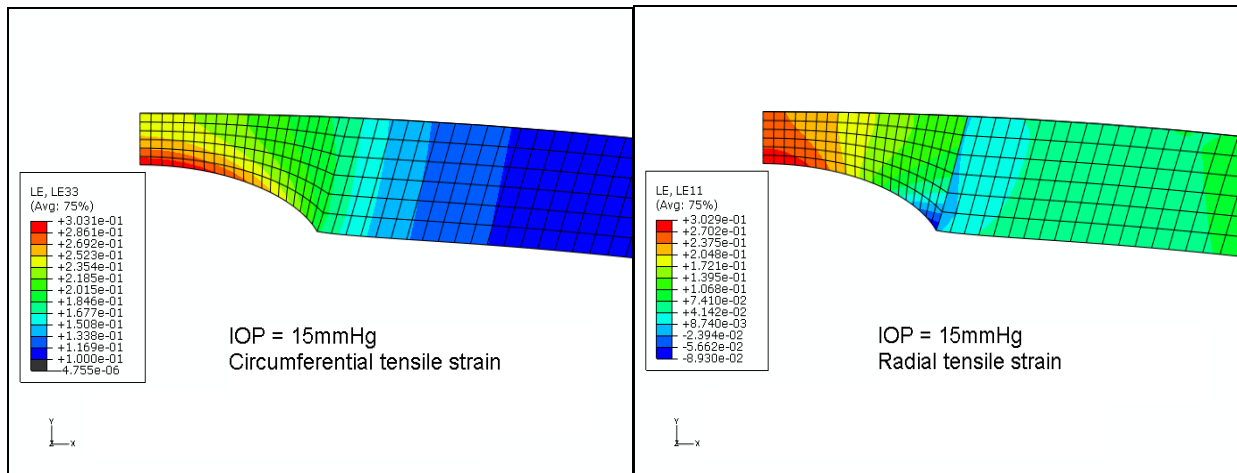
Fig.41. Strain in model-2 at 25 mmHg.

The circumferential strain, Fig.41(left) and the radial strain, Fig.41(right) were maximum at the fovea. The maximum strain was 0.478 in both directions and was located in the inner retinal region of the fovea.
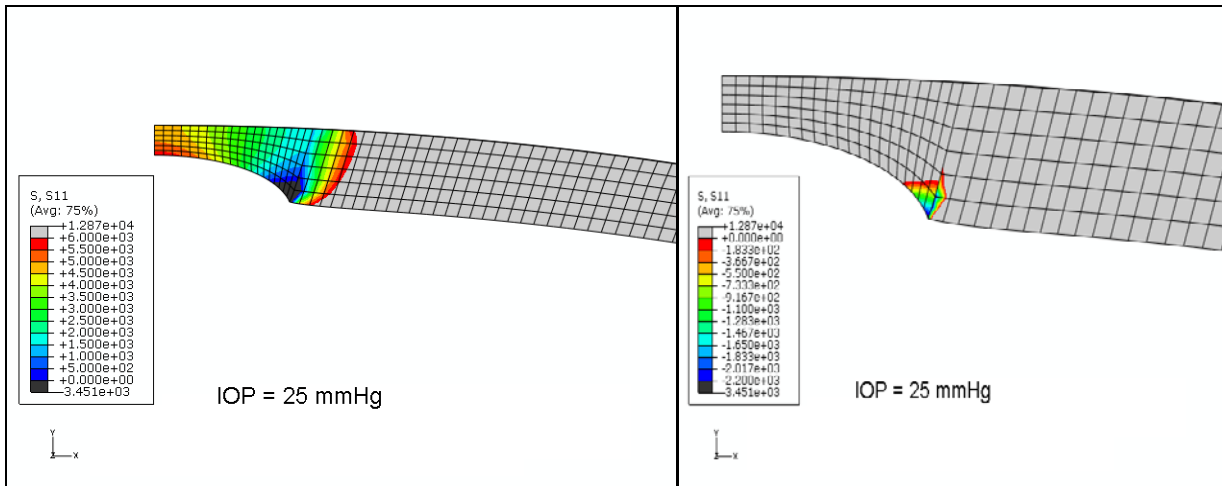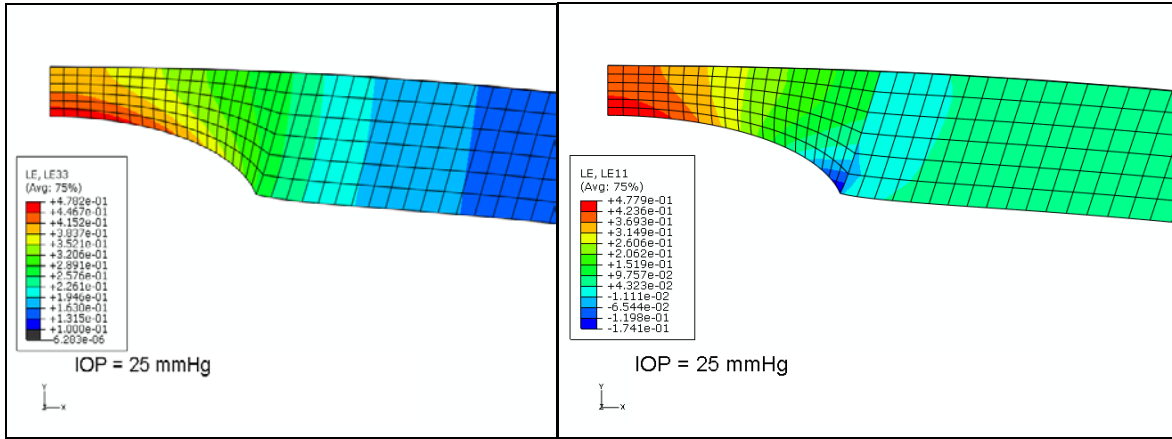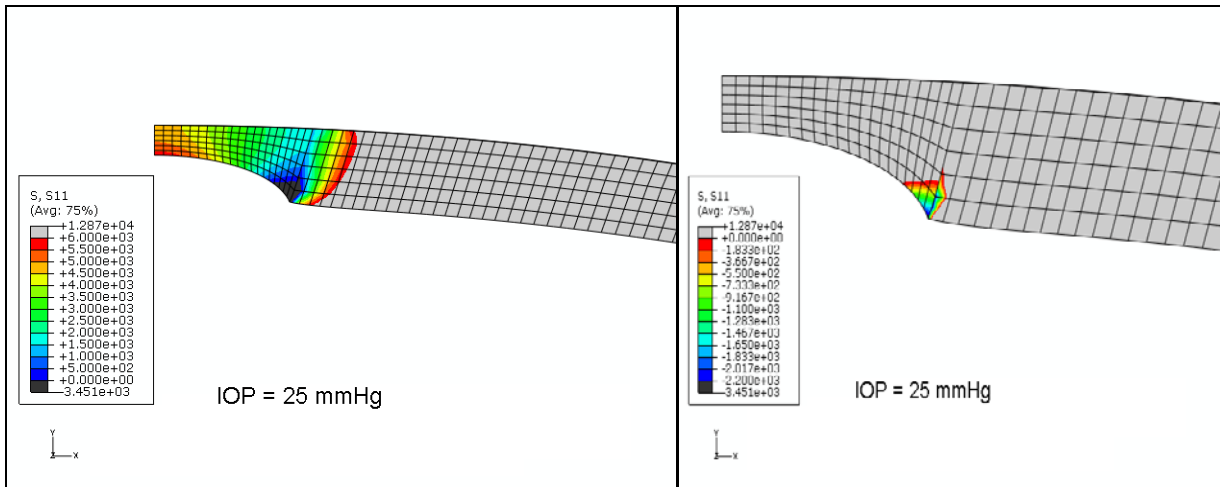

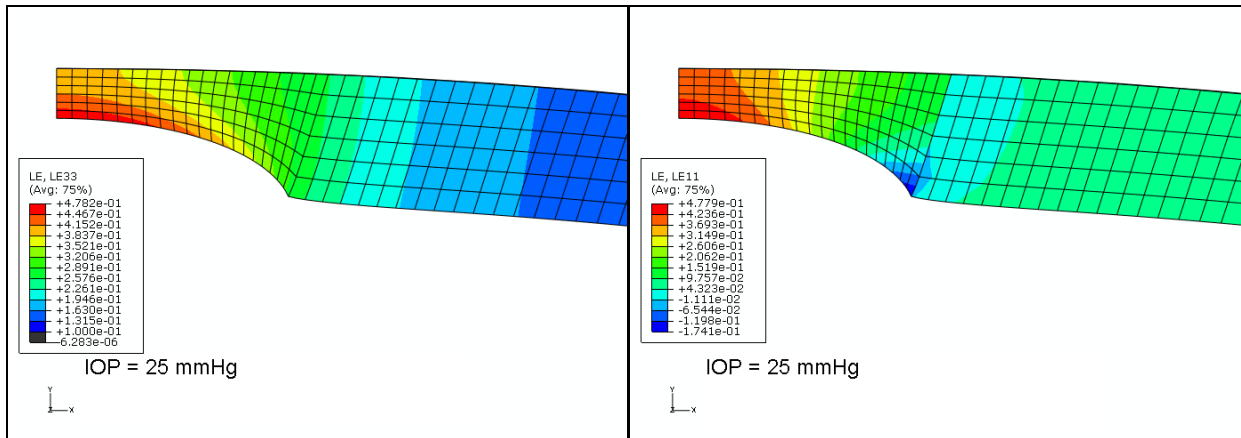Fig.42a. Radial stress in model-2 at 25 mmHg.

Fig.42b. Strain in model-2 at 25mmHg.

The radial tensile stress showed a region of reduced stress near the border of the fovea and the retina, Fig.42a (left). The radial stress was 6 kPa at the center of the fovea, reduced to 1kPa near the border of the fovea and then increased in the retina. A small region of radial compressive stress was observed at the corner of the fovea with maximum compressive stress of -2.2 kPa, Fig. 42a(right). The circumferential strain, Fig.42b(left) and the radial strain, Fig.42b(right) were maximum at the fovea. The maximum strain was 0.478 in both directions and was located in the inner retinal region of the fovea.

Model 2 : Discussion

The circumferential stress was dominant as it was almost an order of magnitude greater than the radial stress in the foveal region. The Mises stress was comparable to the circumferential stress. The radial strain and circumferential strain were maximum at the center of the fovea. Model-2 also supported the results of Model-1 that the fovea was under high tensile radial and circumferential stress and strain in the central region of the retina. The high strains could cause reducing the density in this region. These changes may result in decreased visual acuity. The compressive strain at the outer edge of the fovea could be a result of stress concentration due to geometric discontinuity at the corner of the fovea. The retina material was modeled to have Mooney-Rivlin hyper-elastic properties based on the results from Wollensak[35] and Springer[9]. The values of the Mooney-Rivlin material constants were evaluated using Abaqus. The value for C_{10} was -11765 and C_{01} was 27000. A negative

value for the Mooney-Rivlin constant may not be physically valid. However negative values for these constants have been noted for biomaterials previously by Hu *et al*[43]. A bilinear model was approximated to fit the data rather than the Mooney-Rivlin model that was used for model 2. The bilinear model had a Yield stress of 8.3 kPa at 0.1 strain.

Model 3 : Results
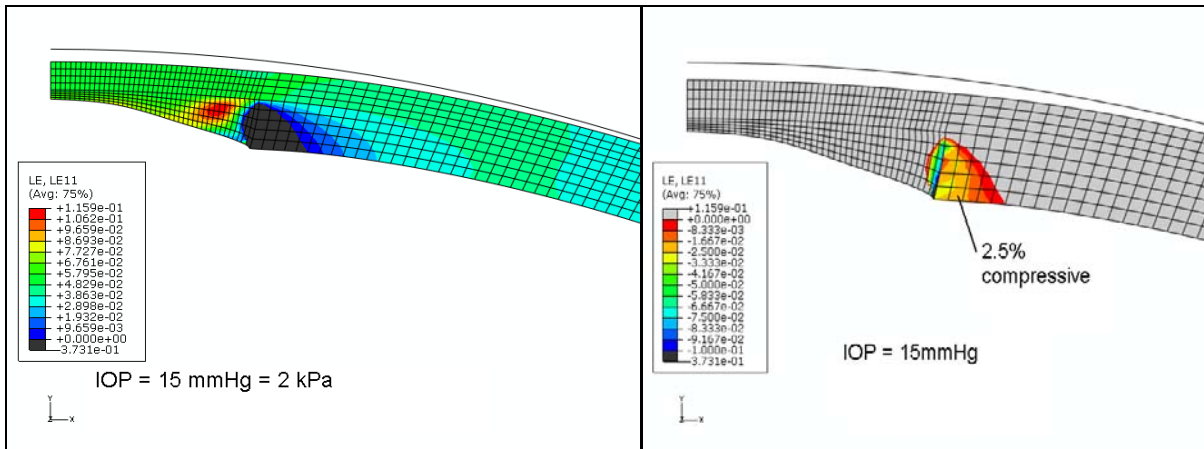
Fig.43a.Radial strain in model-3 at 15 mmHg.
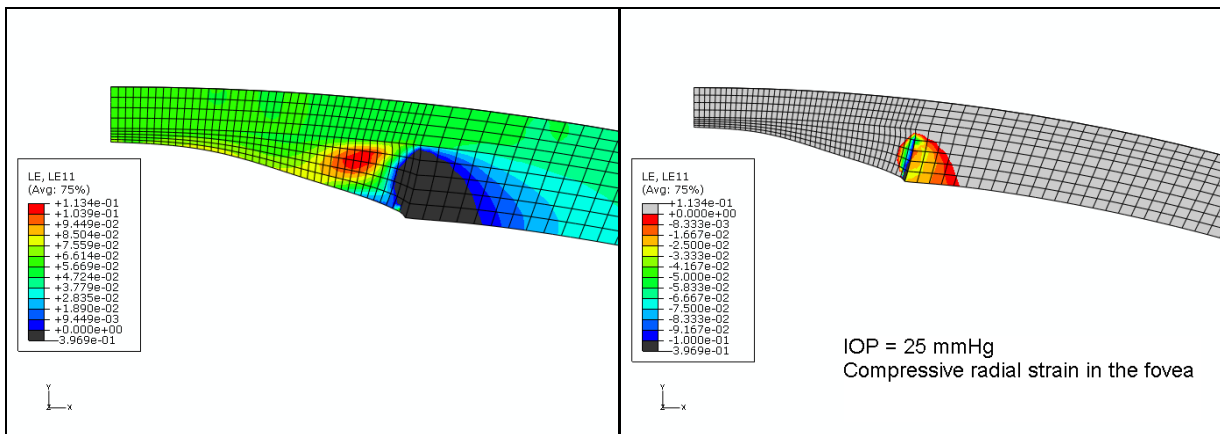
Fig.43b.Radial strain in model-3 at 25 mmHg.

The choroid was not in complete contact with sclera for 15mmHg. The fovea, retina and the choroid were in radial tensile strain due to the applied IOP. The maximum radial tensile strain was 0.11 and located in the fovea, Fig.43a(left). A region of radial compressive strain (0.025) was observed at the border of the fovea and the retina, Fig.43a (right). With increase in IOP to 25mmHg, the choroid made a complete contact with the sclera. The shear stress between the sclera and the choroid was zero as a frictionless contact was defined in the

boundary condition. The radial strain remained as same as observed for the 15mmHg IOP case, Fig.43b.
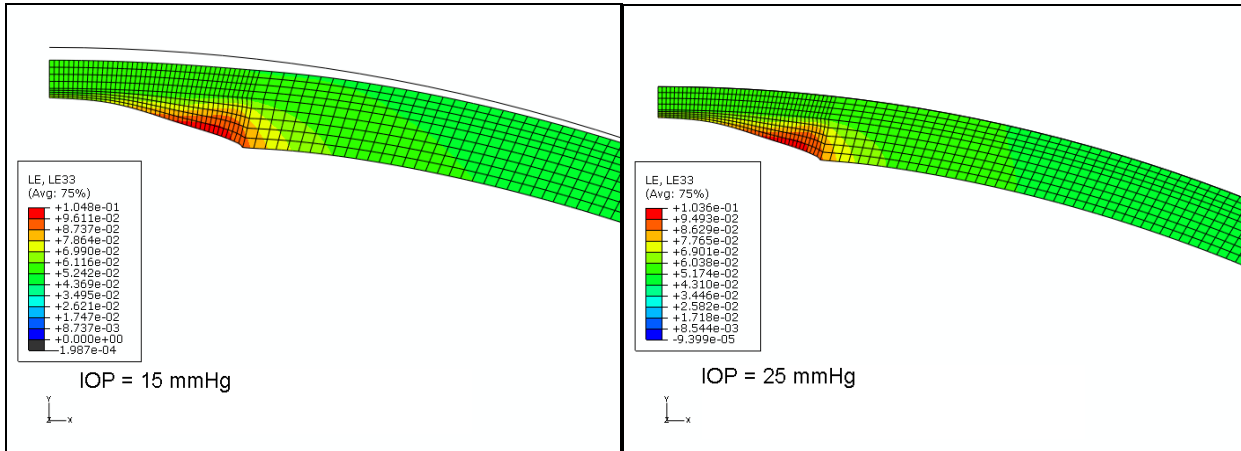
Fig.44.Circumferential tensile strain in model-3.

A tensile circumferential strain was observed in the retina (including the fovea) and the choroid. The maximum circumferential strain of 0.10 occurred at the inner edge of the fovea, near the border with the retina, Fig.44 (left), for 15mmHg IOP. With increase in IOP to 25mmHg the circumferential strain remained same, Fig.44 (right). The maximum radial tensile stress of 70 kPa was observed above the fovea in the choroid region, Fig.45a(left), at 15 mmHg IOP when the choroid was not in complete contact with the sclera. At IOP of 25 mmHg, the region of maximum radial stress was seen at the central outer edge of the choroid, Fig.45a(right).
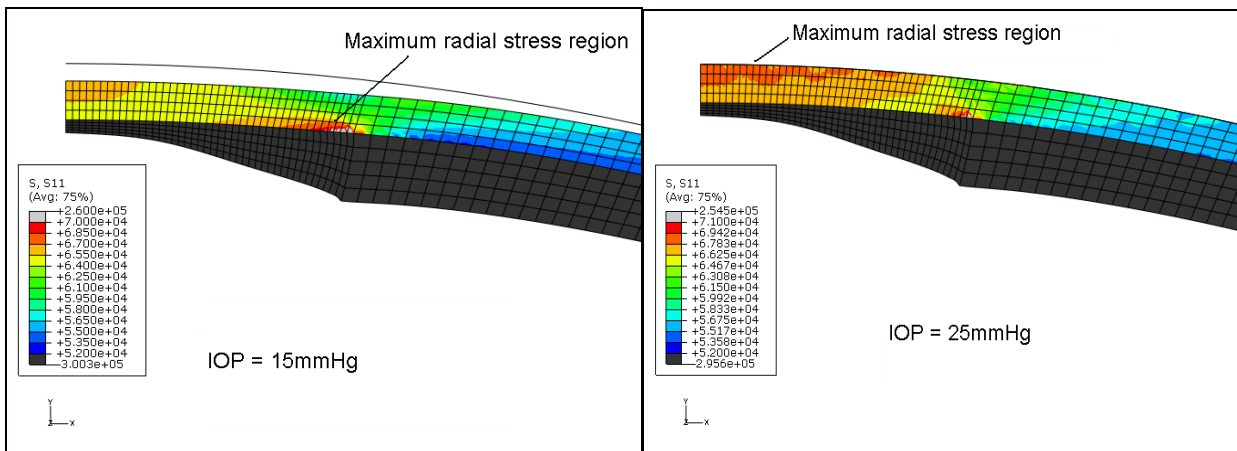
Fig.45a.Radial tensile stress in model-3.
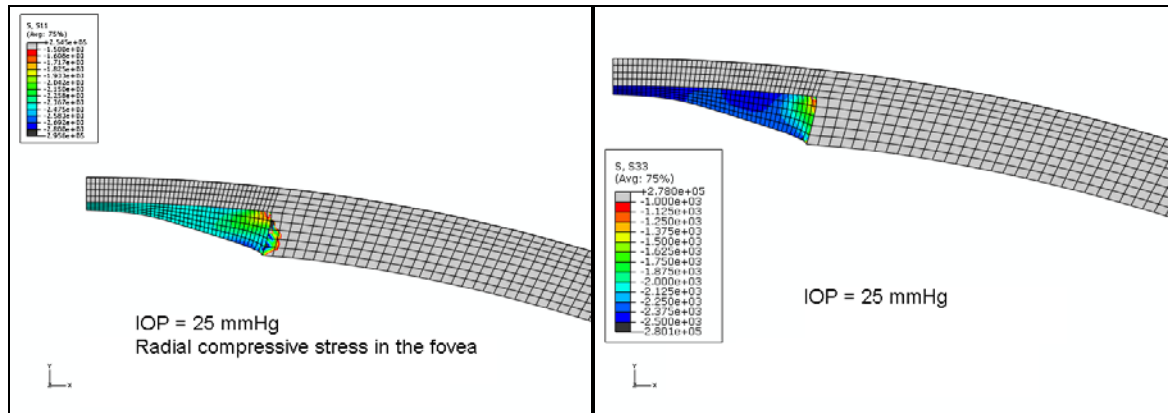
Fig.45b. Compressive stress in model-3.
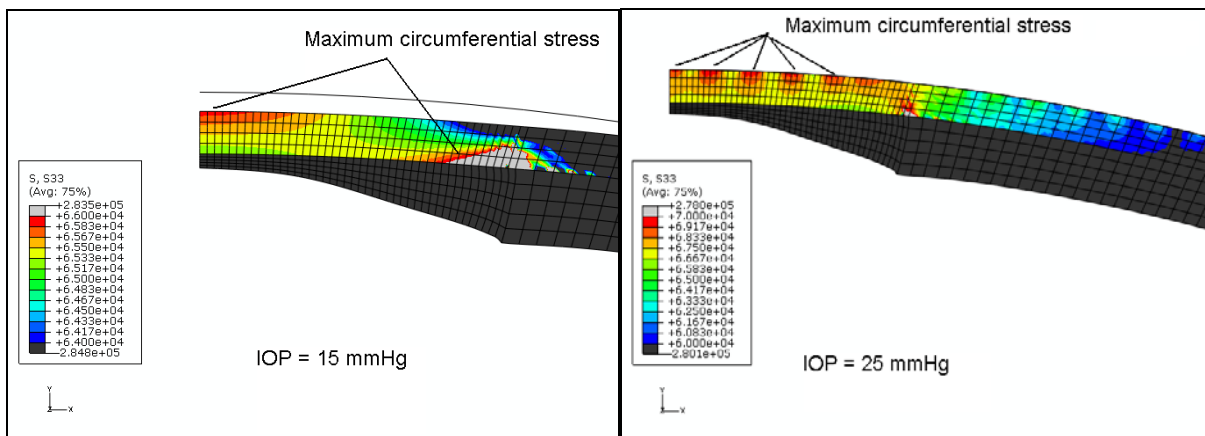
Fig.46.Circumferential tensile stress in model-3.

A compressive radial and circumferential stress is seen in the fovea, Fig.45b. The circumferential tensile stress was maximum in the choroid above the fovea. At 15 mmHg, the maximum circumferential stress of 66 kPa was at the center of the choroid and above the edge of the fovea and retina, Fig. 46 (left). For 25 mmHg IOP, the maximum tensile circumferential stress (70 kPa) was observed in multiple regions along the outer surface of the choroid, Fig. 46 (right).

Model 3 : Discussion

The choroid was stiffer than the retina and thus showed maximum stress in the model. The shear stress on the outer edge of the choroid was zero as a frictionless contact was

defined during modeling. The maximum radial and circumferential strains were as high as 11% in the fovea. The radial strain in the fovea indicates a possible centrifugal movement of the retinal cells in the foveal region. This could support the theory of foveal pit formation put forth by Springer[9] . The maximum circumferential strain was observed at the boundary of the fovea and the choroid. This was the region of photoreceptors, RPE and Bruch's membrane. The radial and circumferential stresses at 15 mmHg were maximum in the inner choroidal region where a delicate network choroicapillaries exists. For IOP of 25 mmHg, the effect of concentric regions of high circumferential tensile stress on radial compression should be studied. This could be helpful to evaluate possible wrinkling of the choroid as suggested by Friberg[8]. Adhesive forces present between the sclera and the choroid which would cause shear stress between them should be modeled in the future.

Model 4 : Results

Fig. 47 shows a section of the deformed shape and Mises stress distribution for 15mmHg IOP.
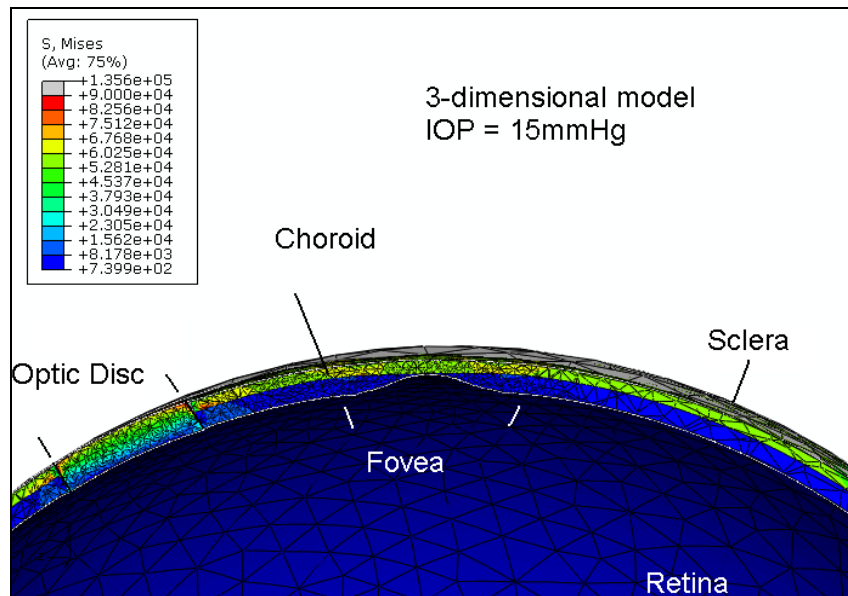
Fig.47.Mises stress in model-4.
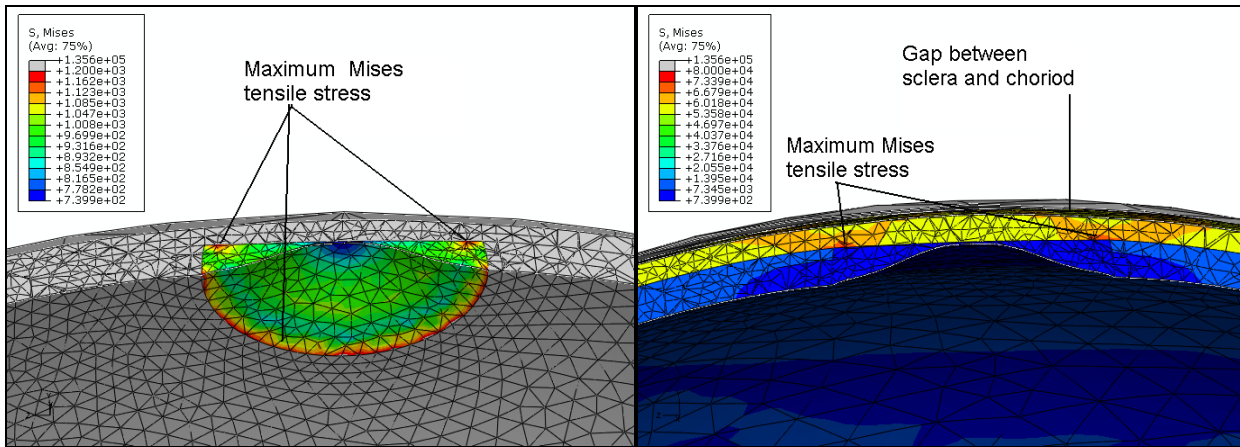
Fig.48.Mises stress in model-4 at 15 mmHg.
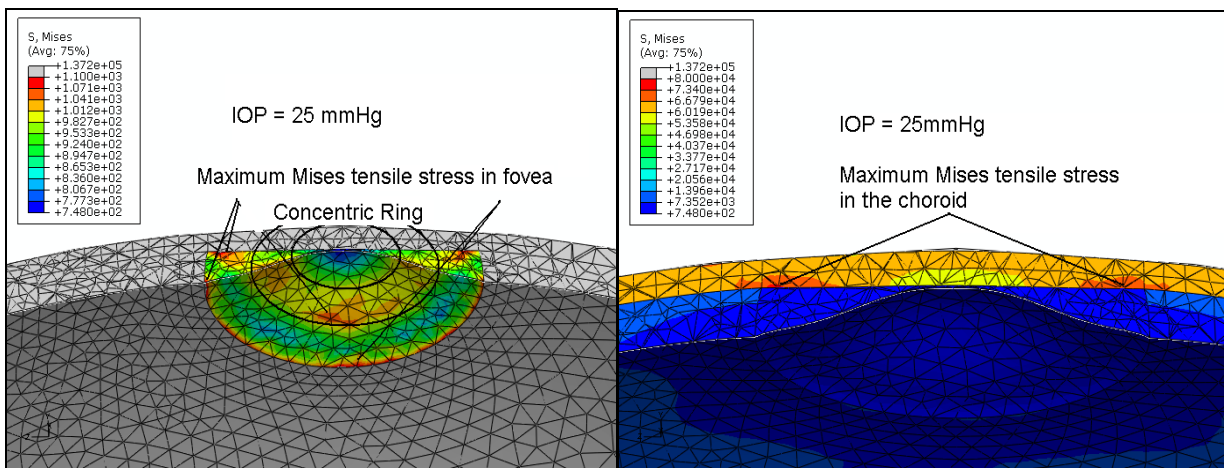
Fig.49.Mises stress in model-4 at 25 mmHg.

The choroid was not in complete contact with the sclera for 15 mmHg IOP.The Mises tensile stress distribution for model 4 at 15 mmHg showed maximum stress (1.2 kPa) at the border of the fovea with the retina and also at the outer edge with the fovea away from the center, Fig.48 (left). This stress reduced gradually to the center of the fovea. The maximum Mises stress (80 kPa) in the choroid was located above the border of the fovea-retina border, Fig. 48 (right). For 25 mmHg IOP, the choroid was in complete contact with the sclera. For 25 mmHg, the maximum tensile Mises stress in the fovea was seen at the fovea-retina border and also at the edge with the choroid away from the center. A concentric ring of high tensile Mises stress was noted in the fovea, Fig.49(left). Maximum Mises stress of 80 kPa was observed in the same location as for the 15mmHg IOP, Fig.49 (right).
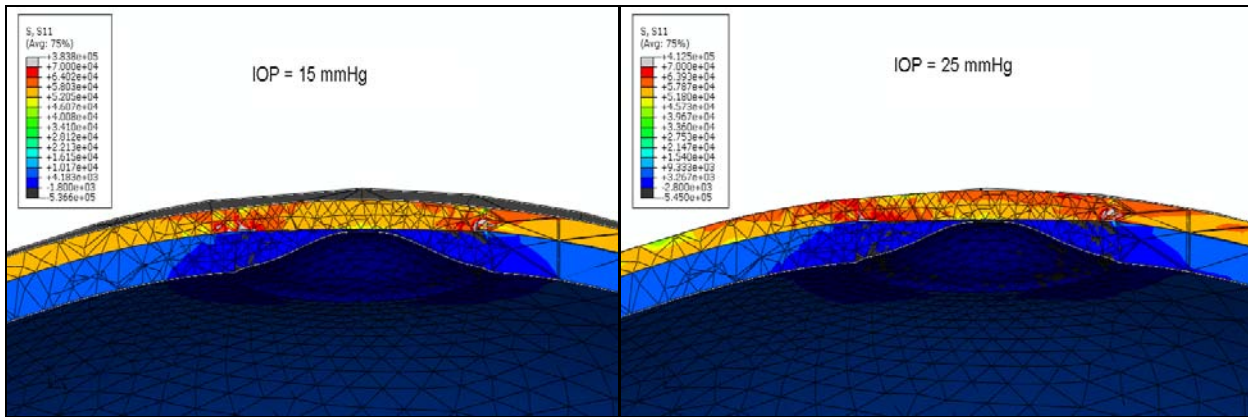
Fig.50. Radial stress in model-4.
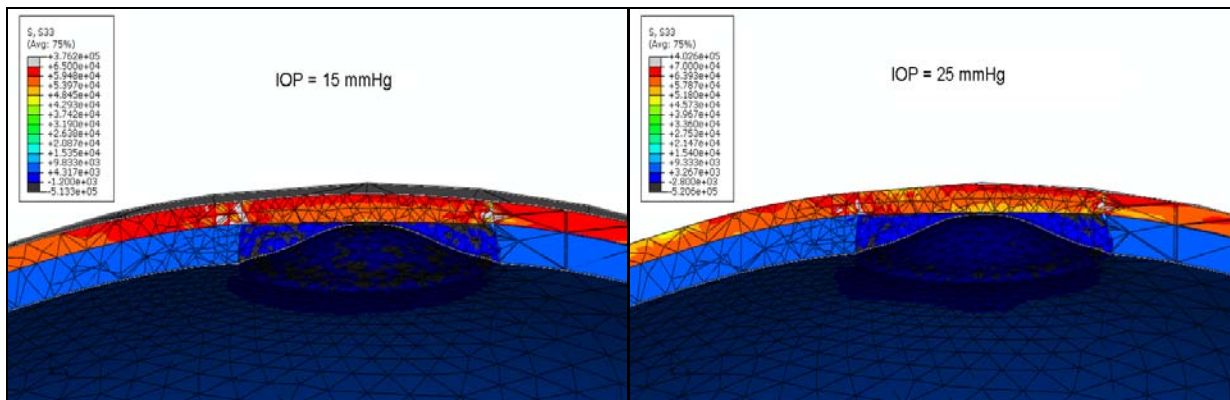
Fig.51. Circumferential stress in model-4.

The radial tensile stress was maximum (70 kPa) in the choroid above the fovea-retina border at 15mmHg, Fig.50 (left). With increase in IOP to 25 mmHg, the magnitude of the stress remained constant, Fig.50 (right). More region of the choroid was now under 70 kPa radial tensile stress. The circumferential stress was maximum above the fovea-retina border in the choroid. For 15mmHg it was 65kPa and increased to 70kPa for 25mmHg IOP, Fig.51. The radial strain was maximum (0.115) in the fovea near the fovea-retina border. As IOP was increased to 25 mmHg, the strain remained the same. A region of compressive strain (0.03) was observed in the retina at the corner of the fovea-retina border, Fig.52.
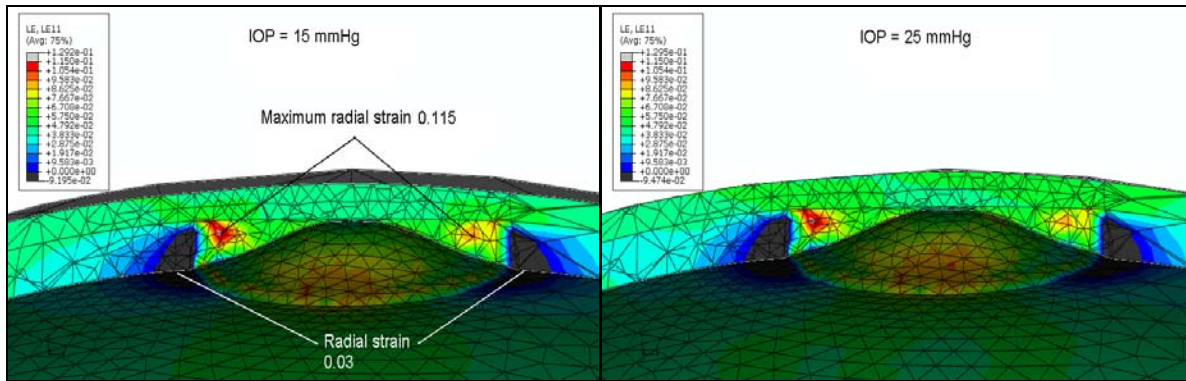
Fig.52. Radial strain in model-4.

The maximum circumferential strain (0.11) was observed at the inner edge of the fovea for 15 and 20 mmHg IOP, Fig. 53.
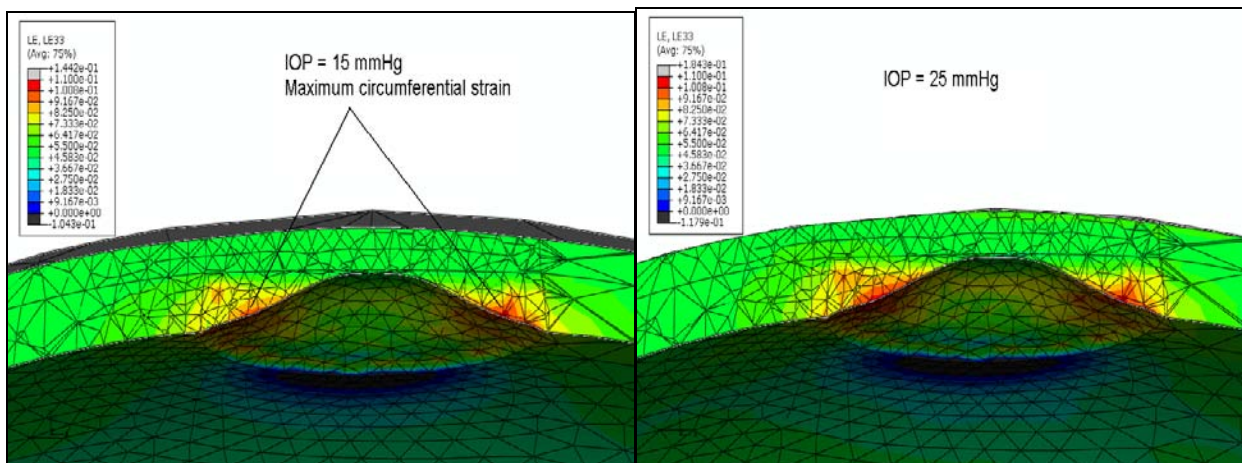
Fig.53. Circumferential strain in model-4.

Model 4 : Discussion

The maximum tensile Mises stress was observed at the border of the retina and fovea in the foveal pit region where there exists a network of retinal vessel capillaries. Also the maximum tensile Mises stress in the choroid was in the region of the delicate choriocapillaries and Bruch's membrane. The concentric high tensile stress regions were qualitatively consistent as previously seen in model 3. The radial tensile stress was maximum above the border of the retina and fovea; a region where neovascularization has been observed during myopic macular staphylomas by Quaranta *et al* [25]. The radial and circumferential tensile strains were 11% as seen in model 3 as well. The tensile radial strain suggests retinal stretching as discussed for model 3. The compressive radial strain was observed due to

63

geometric discontinuity at the corner of the fovea. The circumferential tensile strain was maximum in the inner foveal region also consistent with model 3 results.

Membrane Test : Results
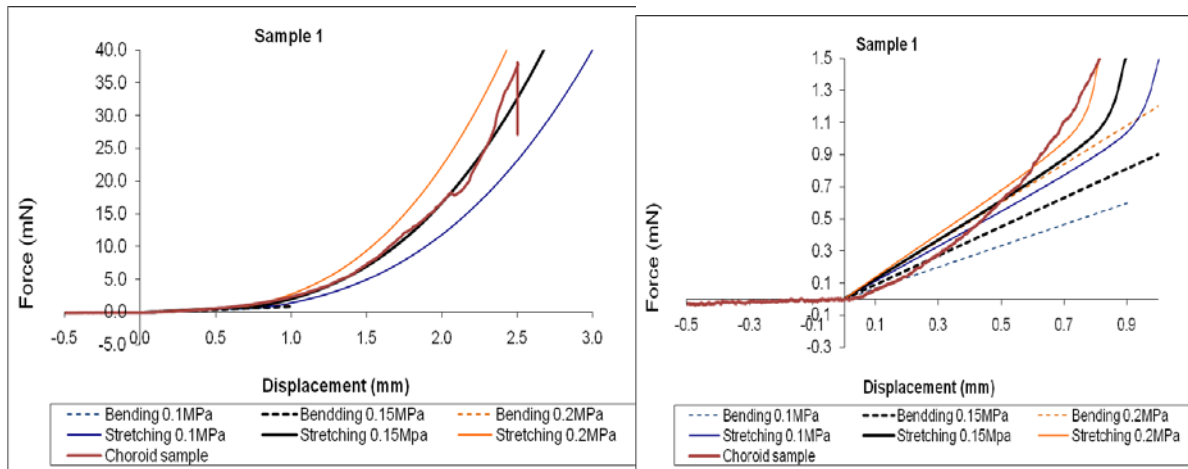
Fig. 54. Force-displacement plot for sample-1 in membrane test.

The force-displacement plot for a choroid sample under a membrane test was obtained from the experiment and fitted with the equation for bending, (21) and equation for stretching, (22) of a circular plate with center point load with elastic modulus of 0.1, 0.15 and 0.2 MPa. The plot for 0.15 MPa modulus was a close fit for the experimental result in the stretching region beyond 1 mm displacement, Fig. 54 (left), where as the plot for 0.1 MPa fitted well in the bending region, Fig. 54 (right). The log plot of the force-displacewment curve showed a transition from bending (slope = 1) to stretching (slope = 3), Fig. 55.
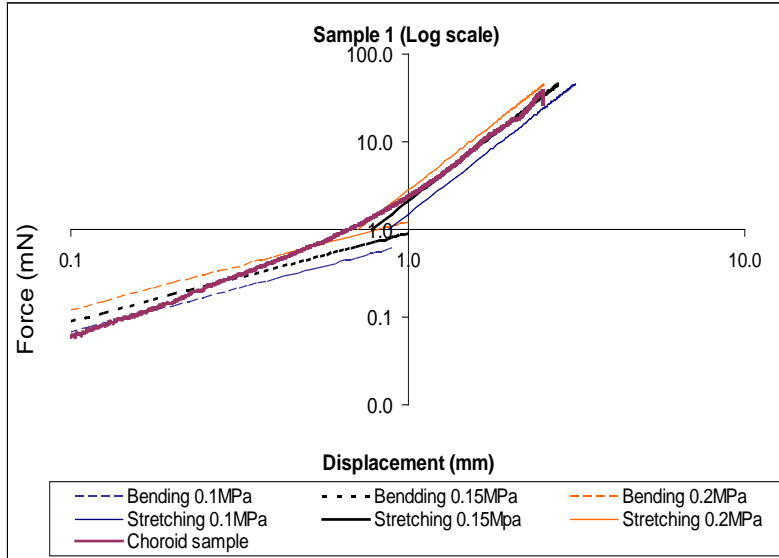
Fig. 55. Log plot of force-displacement plot for sample-1 in membrane test.
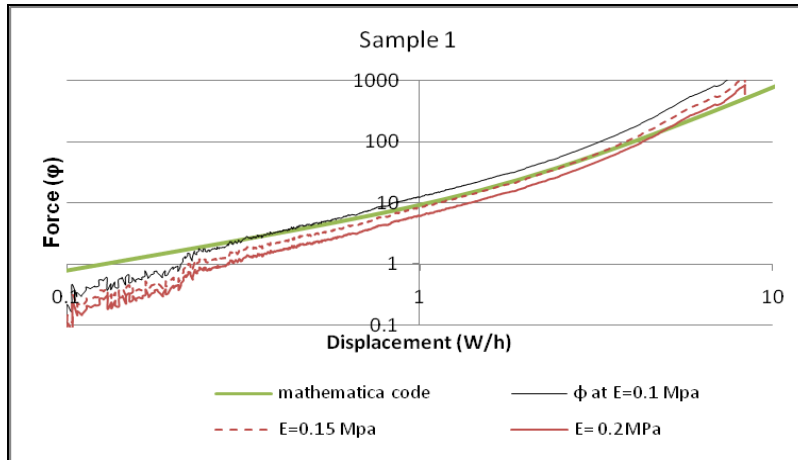
Fig. 56. Transition analysis of sample-1 in membrane test.

The bending-to-stretching transition for thin clamped circular film under an external center point load was given by Wan et al, (23). Elastic modulus of 0.1, 0.15 and 0.2 MPa in the experimental data were used to fit this equation solved using Mathematica (Wolfram Research, Inc.), Fig.56. The transition from 1-slope to 3-slope was seen in this plot. The numerical plot was in the range for elastic modulus of 0.1 to 0.2 MPa. Thus the modulus of the choroid (sample 1) tested using the membrane test was approximated as 0.15 MPa considering bending, stretching and bending-to-stretching analysis. Another sample of the choroid was tested and analysis carried out to calculate the modulus of elasticity in a similar manner. Two tests of loading and unloading cycles were performed on this sample, Fig.57.
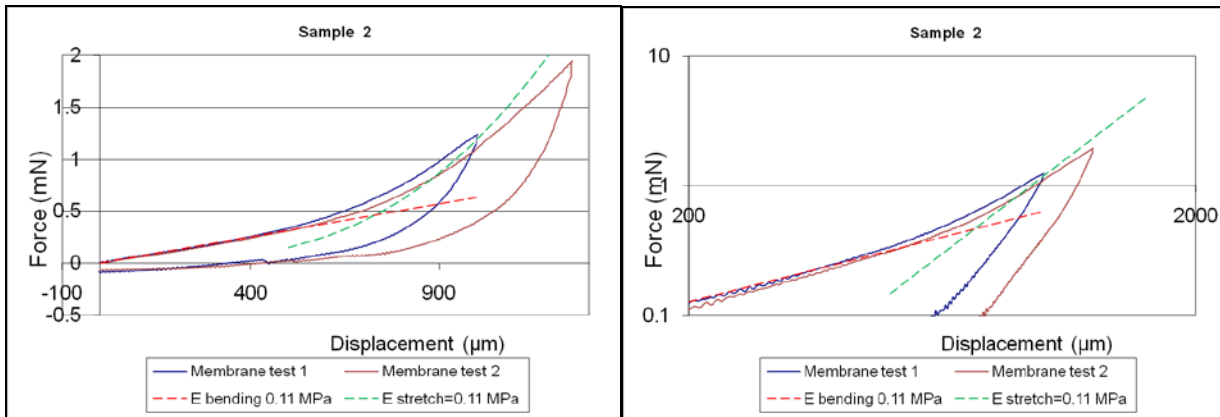
Fig.57. Force – displacement plot for sample-2 in membrane test.

An elastic modulus of 0.11 MPa fitted well for both tests in the bending and stretching analysis. The numerical transition curve, (23) with 0.11 MPa elastic modulus however showed a poor fit in the stretching region, Fig.58(left). Rather a 0.07 MPa modulus for the experimental data fitted more closely with the numerical solution, Fig. 58(right). For further calculation of the elastic modulus, a value of 0.11 MPa was used for the choroid in sample 2. Similar tests were carried out on six more samples and the averaged elastic modulus was 0.2 MPa with standard deviation of 0.08 MPa, Table 2.
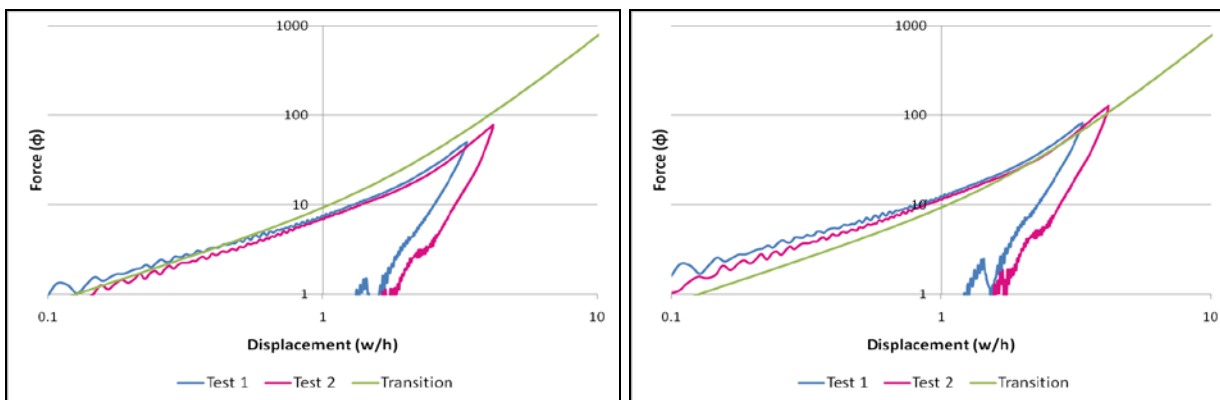
Fig.58. Transition analysis of sample-2 in membrane test.

Table 2. Calculated elastic modulus for the choroid in membrane tests.

	Date	Test 1		Test 2		Force required to indent up to 1mm
		E (Bending)	E (Stretching)	E (Bending)	E (Stretching)	
		MPa	MPa	MPa	MPa	mN
sample 1	24 Feb #1	0.1	0.15	0.05	0.1	2
sample 2	14 May #2	0.11	0.11	0.11	0.11	1.2
sample 3	18 Mar #2	0.4	1	0.2	0.7	12
sample 4	13 May #1	0.25	0.5	0.25	0.5	6
sample 5	13 May #2	0.1	0.15	0.07	0.1	1.2
sample 6	14 May #1	0.1	0.15	0.1	0.15	1.8
sample 7	18 Mar #1	0.125	0.3	0.125	0.3	2
sample 8	14 May #3	0.05	0.05	0.05	0.03	0.4
	Average	0.154375	0.30125	0.119375	0.24875	3.325
	E avgeraged	0.205938				
	Std. dev.	0.083804				

Tensile test : Results

The choroid was also tested in uniaxial tension at rates of 10, 100and 1000µm/s for 3%, 10% and up to failure. The results for the tensile test showed a linear curve on the stress-strain plot for 10 µm /s rate and up to 3% strain, Fig.59 (left). The first loading curve tended to change slope at 0.017 strain approximately. The sample was further loaded and unloaded five times at same rate and elongation. The loss of energy between the loading and unloading in test 1 was wide as compared to the next five tests. Tests 2 – 5 were consistent compared to test 1. The slope of all the tests up to 1.5% strain was 350 kPa (0.35 MPa). Sample 4, was tested at rate 10 µm /s upto 10% strain showed an elastic modulus of 0.33MPa for small strain (3%), Fig.59 (right).
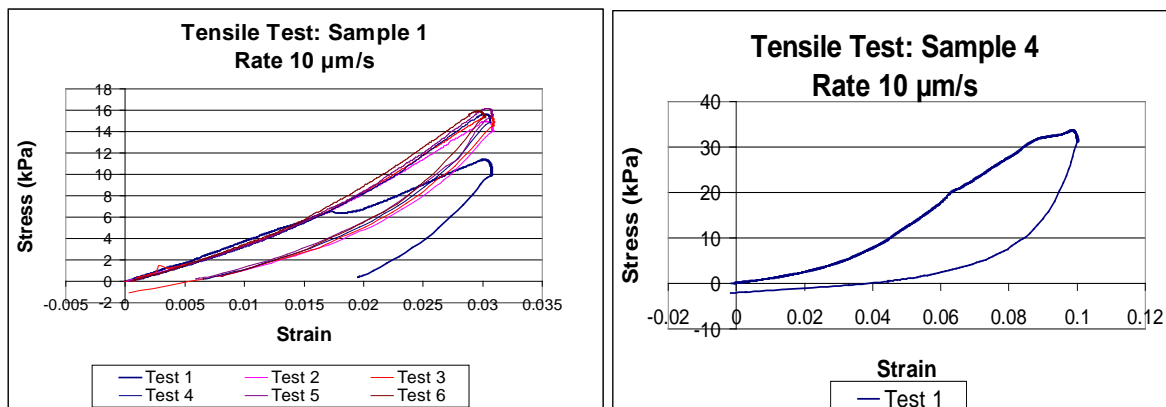
Fig.59a. Stress strain plot of tensile test at 10 µm/s rate.
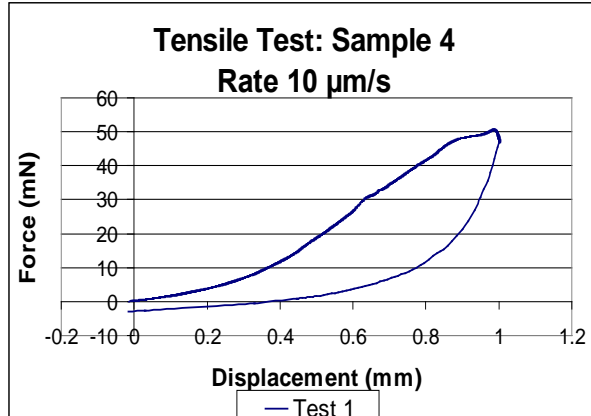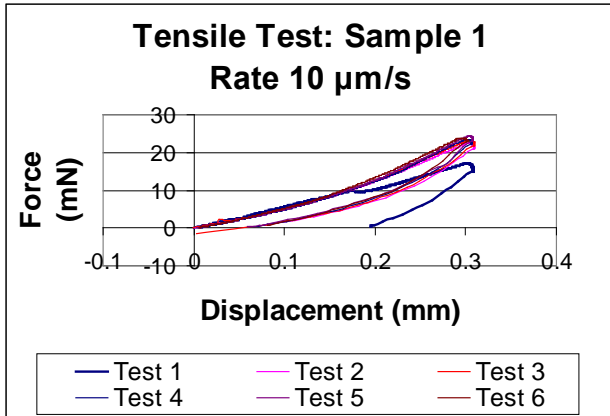
Fig.59b. Force displacement plot of tensile test at 10 µm/s rate.
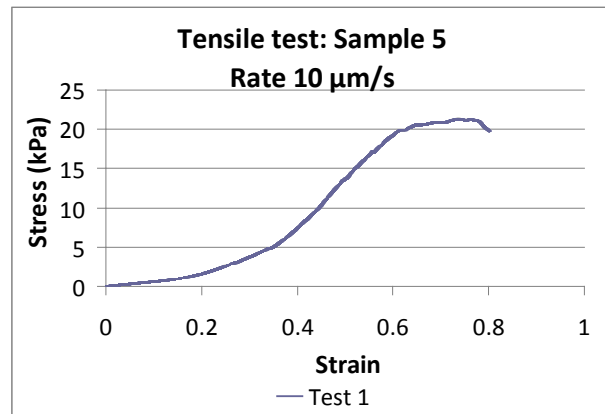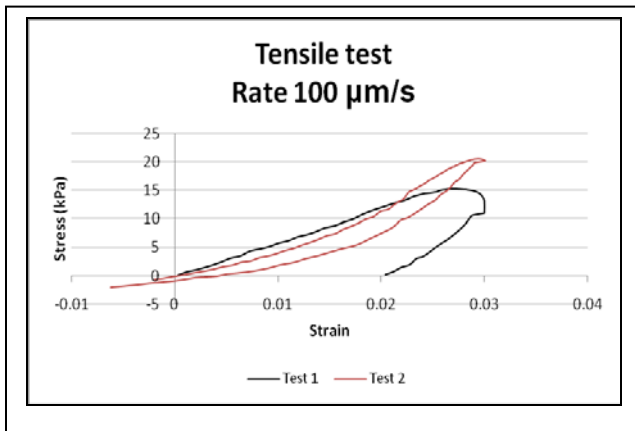
Fig.60a. Stress strain plot of tensile test at 10 µm/s and 100 µm/s rate.
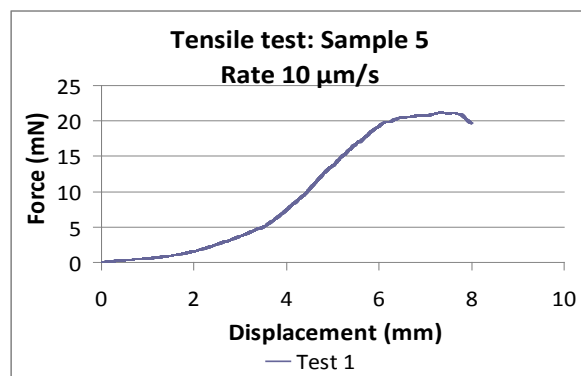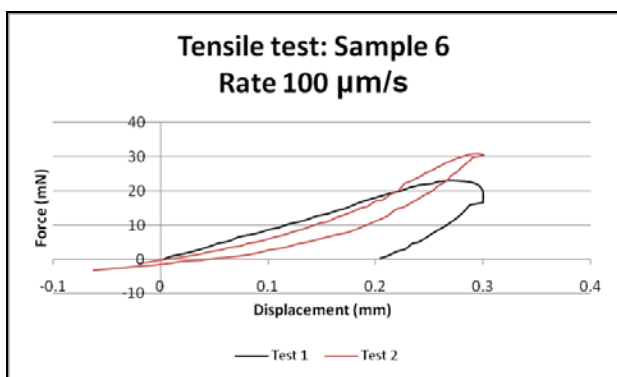
Fig.60b. Force displacement plot of tensile test at 10 µm/s and 100 µm/s rate.

The choroid when tested to failure at 10 µm /s rate had a modulus of 5.5kPa upto 0.1 strain Fig. 60 (left) and the sample broke at 0.8 strain. Another choroid sample tested at

10µm/s up to 3% strain showed a modulus of 575kPa in Test 1 and 440 kPa in Test 2, Fig. 60 (right).

Table 3. Calculated elastic modulus for the choroid in uniaxial tensile tests.

(Shaded region excluded from further calculation)

Rate (µm/s)	Max. Strain	Max. Stress (kPa)	E (kPa)	2nd test	3rd	4th	5th	6th
	3%	16	350	350	350	350	350	350
		19	420	420	420	420		
10		16	300	300	300			
	10%	38	330					
	80%	21	5.5					
	3%	20	575	440				
100	10%	60	500					
	15%	12	20					
500	3%	1.2	20	35			Avg.	383.8235
1000	22%	100	140				S.Dev.	74.69792

The choroid was tested in uniaxial tesion for various strain rates and up to different strains as shown in a summary of results. The elastic modulus for each test is shown in Table 3. The results in the shaded region of Table 3 were neglected during further calculation as they indicated lower elastic modulus than previously noted (0.2 to 0.8MPa)[37]. The averaged elastic modulus of the choroid calculated based on the uniaxial tension testing was 0.383 MPa with a standard deviation of 0.074 MPa.

11. Future work

The 3-Dimensional model presented should be developed in the future. A dense meshing in the central region of the retina should be utilized for more qualitative results. The shear forces between the retinal and choroidal layers should be studied to understand the changes in anatomy and related physiology and pathological changes. The corner of the fovea should be modeled considering the details of the anatomy of the eye to avoid stress concentrations. Experiments have been performed by Zauberman[48] to determine the adhesive forces acting between the retina and the choroid. The results can be used in modeling the future FE models. The adhesion between the sclera and choroid should also be modeled to realistically simulate the eye. The optic disc in the 3-D model needs more careful modeling for geometry and material properties. The optic nerve connecting the retina through the optic canal would induce stress in the fovea. The retina and the choroid do not have any physical connections and the retina seems to slide freely over the choroid. This would considerably alter the modeling approach and the stress field in this case should be studied and compared with the results of this study. The attachment of the retina at the ora serratta (edge) should be modeled more accurately. This would enable the study of accommodation induced retinal stretch in myopia. This study includes the effect of material properties and IOP in the central retina with fixed axial length. Future studies could include increasing the axial length gradually to study the effects of progressive axial myopia on the central retinal region.

Membrane test

The membrane tests on the choroid have enabled to calculate the elastic modulus to be 0.2 MPa. The estimates of the elastic modulus depend on the experimental procedure as well as curve fitting and mathematical calculations. A microscopic imaging of the choroid being tested should be carried out to determine specifically the layers of the choroid (Bruch's membrane, choriocapillaries, intermediate or large vessel layer) being tested. The dimensions of the specimen were approximately measured using a micrometer and a vernier caliper. The thickness measurement needs careful attention as the micrometer might compress it and damage the specimen. The saline solution used for the test used was at room temperature

(22°C). This solution should be at body temperature (37°C) to simulate in vivo conditions and have more realistic results. An imaging technique needs to be developed for the present experimental setup to get images of the deformation of the membrane being tested. This will help in data analysis and also detect the exact start point of the test and slippage of the specimen.

Tensile Test

The elastic modulus of the choroid based on the tensile tests was calculated to be 0.383MPa. The results in the shaded region were excluded from the calculation as they were lower than the expected range. Some reasons for the inconsistency of the results of the tensile test could be as follows:
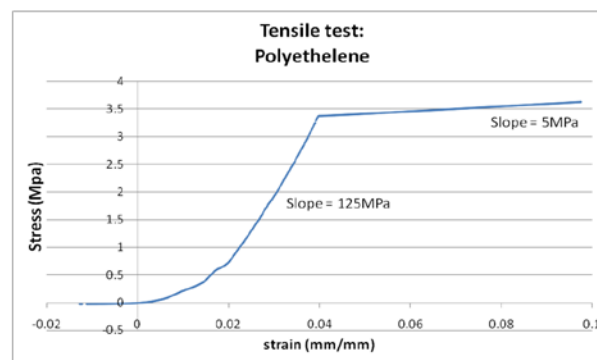
Polyethylene : Length =8.5mm, width =4mm , thickness =25micron ,
Poisson's ratio =0.3, Elastic modulus ≈200MPa

Fig.61a. Tensile test of polyethylene.
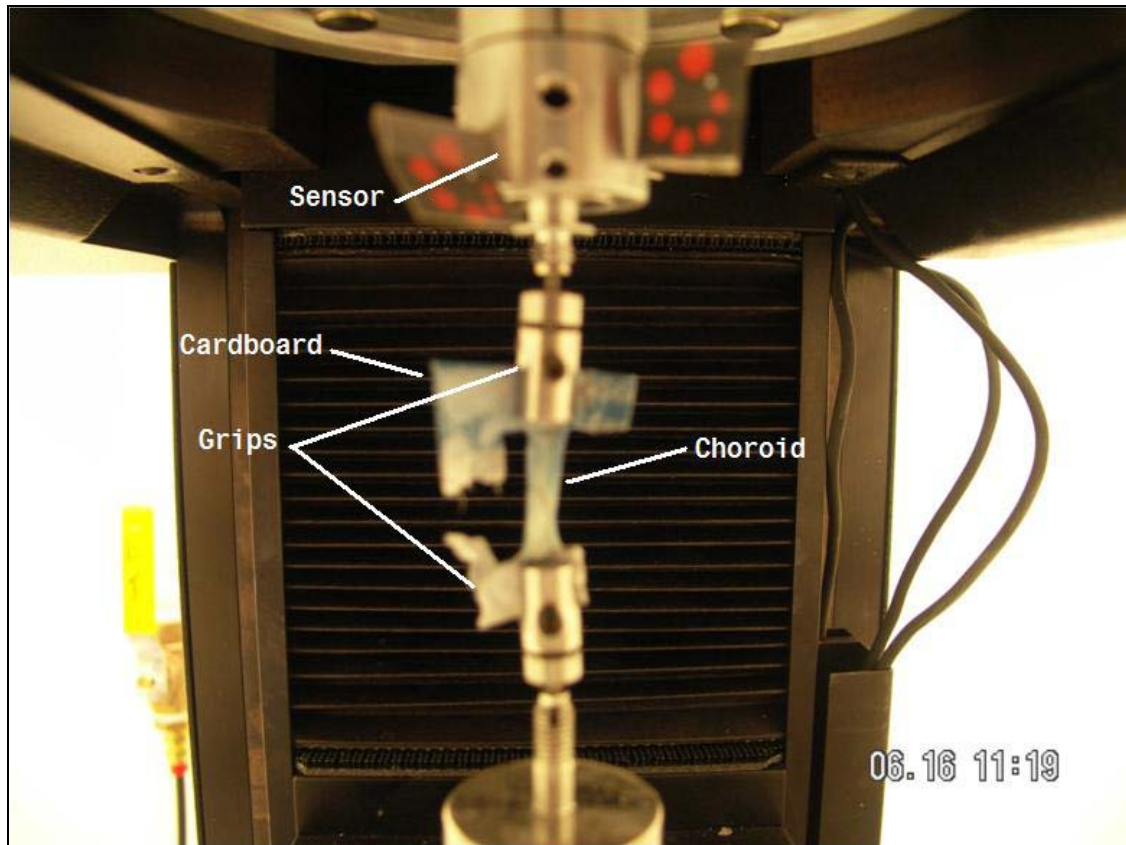
Fig.61b. Tensile test of choroid.

The tensile test on the choroid was carried out in air. Instead it should be carried out in a humid chamber at 37° C. The alignment of the clamps to grip the choroid specimen should be collinear to obtain a uniaxial tension system. A similar tension test was carried out on Low Density Polyethelene, Fig.61a. The elastic region showed a parabolic curve instead of a straight line up to yielding. This suggests some sort of misalignment during experimentation. The cardboard frame used to hold the choroid in place during setup of the experiment showed a slanting lower half during the experiment, Fig.61b. An imaging technique should be used for the current experimental setup to detect any slippage during the test.

Experimentation to calculate the physical properties of the choroid and retina should be carried out in the future. The numerical models (21,22,23) assume a linear elastic material model and their use is questionable to estimate the properties of the choroid. A hyper-elastic model will be more suited to evaluate the properties of such biological tissues. The retina in the

eye was exposed to biaxial stresses as previously noted. Biaxial loading experiment would be of more value and realistic to determine the failure criterion for the retina. Holerfin *et al* [49] developed a biaxial tensile testing device, experimentally determined crystallographic yield loci and compared them to yield stresses and the ratio of plastic strains to the Taylor-Bishop-Hill model. This will enable the modeling of the eye and study the biomechanics involved in the pathology of a number of diseases. It will also help in the manufacturing of prosthetic replacements of these tissues.

12. Conclusion

The mechanics of the retina and choroid in a high myopic eye were investigated using Finite Element Analysis. FEA has traditionally been utilized to study the ocular structure. Basic knowledge of the mechanical properties, anatomy and physiology is required to perform the analysis and apply FEA results to biological structures to draw meaningful conclusions. Knowledge of pathogenesis is also necessary to understand the significance of the observed stress, strain and their location. This study suggested that the fovea was under maximum radial and circumferential stress in the myopic eye. Strain of 11% was predicted in the foveal region indicating stretching of this region. A conventional engineering material would exhibit plastic deformation beyond the yield point in axial loading. Von Mises stress criterion is used to determine the behavior of conventional engineering materials (metals) in multi axial loading beyond the yield point. However Von Mises criterion is not a dependable indicator of plasticity of biological samples. Substantial proof is required for the applicability of Von Mises stress criterion to determine the behavior of biological samples under multi axial loading. Alternatively, a new yield criterion may be developed for biological samples under multi axial loading. Thus the strains of 11% in the foveal region do not indicate whether the retina deforms plastically.

The elastic modulus of the choroid was experimentally evaluated (0.2 ±0.08 MPa)using tensile and membrane tests. The force-displacement plot obtained from the numerical models for the membrane test was fitted to the plot obtained from experimental data. The numerical models assumed a linear elastic modulus. The behavior of biological tissues is non-linear and a numerical model with nonlinear elastic modulus (hyper-elastic) would be appropriate and realistic in evaluating material properties of biological tissues.

The FEA model developed in this study is highly versatile and applicable to a wide range of myopic eye research. The model was based on knowledgeable inputs including realistic geometry, material properties, intra-ocular pressure and boundary conditions. The model can be developed further to reveal the mechanical factors driving the degenerative changes such as choroidal folds, staphyloma, lacquer cracks, myopic crescent in a progressive high myopic eye. With some alterations, the finite element model of the eye can also be used for examining the effects of glaucoma, accommodation, hyperopia and similar ocular diseases on the retina.

References

1. Bell, G.R., *Biomechanical considerations of high myopia: Part II - Biomechanical forces affecting high myopia.* Journal of American Optometric Association, 1993. **64**(5): p. 339-345.
2. Ohno-Matsui, K., Tokoro,T., *The progression of lacquer cracks in pathologic myopia.* Retina., 1996. **16**(1): p. 29-37.
3. Friedman, B., *Stress upon the ocular coasts:effects of scleral curvature, scleral thickness and introcular pressure.* EENT, 1966. **45**(9): p. 59-66.
4. Greene, P.R., *Mechanical considerations in myopia:Relative effects of accommodation, convergence, intraocular pressure, and the extraocular muscles.* American journal of optometry and physiological optics, 1980. **57**(12): p. 902-914.
5. Greene, P.R., *Stress amplification and plastic flow for spheroidal shells:Applications to myopia.* Rheologic Acta, 1987. **26**: p. 479-484.
6. Perkins, E.S., *Myopia and scleral stress.* Doc Ophthalmol Proc Ser, 1981. **28**.
7. Crane, H.D., *Switching properties in bubbles, balloons, capillaries, and alveoli.* Journal of biomechanical engineering, 1973. **6**: p. 411-12.
8. Friberg, T.R., *The etiology of choroidal folds. A biomechanical explanation.* Graefe's archive for clinical and experimental ophthalmol., 1989. **227**(5): p. 459-464.
9. Springer, A.D., Hendrickson, A. E., *Development of the primate area of high acuity.1 Use of finite element analysis models to identify mechanical variables affecting pit formation.* Visual Neuroscience, 2004. **21**: p. 53-62.
10. Sigal, I.A., Flanagan,J.G., Tertinegg,I.,Ethier,R.C., *Finite element modeling of optic nerve head biomechanics.* Investigative Ophthalmology & Visual Science, 2004. **45**: p. 4378-4387.
11. Sigal, I.A., Flanagan,J.G., Tertinegg,I.,Ethier,R.C., *Predicted extension, compression and shearing of optic nerve head tissues.* Experimental eye research, 2007. **85**: p. 312-322.
12. Bellezza, A.J., Hart,R.T., Burgoyne,C.F., *The optic nerve head as a biomechanical structure: Initial finite element modeling.* Investigative Ophthalmology and Visual Science, 2000. **41**: p. 2991-3000.
13. Ljubimova, D., Eriksson,A., Bauer,S., *Aspects of eye accomodation evaluated by finite elements.* Biomechan Model Mechanobiol, 2008. **7**: p. 139-150.
14. Finchman, E.F., *The mechanism of accomodation* British Journal of Opthalmology, 1937. **8**: p. 5-80.
15. Wan, K.-T., Ravi,N., *Mechanics of ocular lens accommodation consistent with the classical Helmholtz theory.* Int. J. Experimental and computational biomechanics, 2009. **in press**.
16. Klein, R.M., Curtin, B.J., *Lacquer crack lesions in pathologic myopia.* American journal of ophthalmology, 1975. **79**(3): p. 386-92.
17. Shapiro, M., Chandra,S.R., *Evolution of lacquer cracks in high myopia.* Annals of ophthalmology., 1985. **17**(4): p. 231-235.

18. Bron, A.J., Tripathi,R.C., Tripathi,B.J., *Wolff's Anatomy of the eye and orbit*. 8 ed. 1997: Chapman and Hall Medical.

19. Enoch, J.M., *Marked accommodation, retinal stretch, monocular space perception and retinal receptor orientation.* American journal of optometry and physiological optics, 1975. **52**: p. 376-392.

20. Hollins, M., *Does the central human retina stretch during accommodation?* Nature, 1974. **251**: p. 729-730.

21. Gariano, R.F., Kim, C-H., *Evaluation and Management of Suspected Retinal Detachment.* American Family Physician, 2004. **69**: p. 1691-8.

22. Curtin, B.J., Karlin,D.B., *Axial length measurements and fundus changes of the myopic eye. I. The posterior fundus.* Trans Am Ophthalmol Soc., 1970. **68**: p. 312-334.

23. Curtin, B.J., *The posterior staphyloma of pathologic myopia.* Trans Am Ophthal Soc, 1977. **75**: p. 67-86.

24. Hsiang, H.W., Ohno-Matsui,K., Shimada,N., Hayashi,K., Moriyama,M., Yoshida,T., Tokoro,T., Mochizuki,M., *Clinical characteristics of posterior staphyloma in eyes with pathologic myopia.* American journal of ophthalmology, 2008. **146**(1): p. 102-110.

25. Quaranta, M., Brindeau,C., Coscas,G., Soubrane,G., *Multiple choroidal neovascularizations at the border of a myopic posterior macular staphyloma.* Graefe's archive for clinical and experimental ophthalmol., 2000. **238**: p. 101-103.

26. Jaeger, E.A., *Miscellaneous diseases of the fundus*, in *Clinical Ophthalmoogy.* 1983, Harper and Row: Philadelphia. p. 1-19.

27. Ohno-Matsui, K., Tokoro,T., *Subretinal bleeding without choroidal neovascularization in pathologic myopia: A Sign of New Lacquer Crack Formation.* Retina, 1996. **16**(3): p. 196-202.

28. Li, H., Wen,F., Wu,D., Luo,G., Huang,S., Guan,T., Liu,C., *Fundus analysis and visual prognosis of macular hemorrhage in pathological myopia without choroidal neovasculopathy.* Eye science, 2004. **20**(1): p. 57-62.

29. Yip, L.W., Eong,K-G. A. , *Recurrent subretinal haemorrhages and progressive lacquer cracks in a high myope.* Acta Ophthalmol. Scand., 2003. **81**: p. 646-647.

30. Cavallerano, A.A., *Lacquer cracks.* Clin. eye vision care, 1991. **3**(4): p. 190-193.

31. Hirata, A., Negi,A., *Lacquer crack lesions in experimental chick myopia.* Graefe's archive for clinical and experimental ophthalmology. , 1998. **236**: p. 138-145.

32. Read, G., *An application of elementary calculus to balloons.* Europ J Physics 1986. **7**: p. 236-41.

33. Timoshenko, S.P., Gere, J. M., *Buckling of thin plates*, in *Theory of elastic stability.* 1961, McGraw- Hill: New York. p. 348-439.

34. Stevens, J.D., Jones, I.L, Warner, M., Lavin, M.J., Leaver, P.K., *Mathematical modelling of retinal tear formation: Implications for the use of heavy liquids.* Eye, 1992. **6**: p. 69-74.

35. Wollensak, G., Spoerl,E., *Biomechanical characteristics of retina.* Retina, 2004. **24**(6): p. 967-970.

36. Jones, I.L., Warner,M.,Stevens,J.D., *Mathematical modelling of the elastic properties of retina: A determination of Young's modulus.* Eye, 1992. **6**: p. 556-559.

37.   Friberg, T.R., Lace,J.W., *A comparison of the elastic properties of human choroid and sclera.* Experimental eye research, 1988. **47**(3): p. 429-436.

38.   Phillips, J.R., McBrien, N. A., *Form deprivation myopia: elastic properties of sclera.* Ophthal. Physiol. Opt., 1995. **15**(5): p. 357-362.

39.   Woo, S.L., Kobayashi,A.S., Schlegel,W.A., Lawrence,C. , *Nonlinear material properties of intact cornea and sclera.* Experimental eye research, 1992. **14**: p. 29-39.

40.   Springer, A.D., D.J.H. Kauffmann, H.Diener, *Finite element analysis (FEA) of retinal stretch during development.* Investigative Ophthalmology & Visual Science, 1995. **36**(4): p. S60.

41.   Ogden, R.W., *Elasticity*, in *Non-Linear Elastic Deformations* 1984, Halsted Press: New York. p. 169-229.

42.   *Hyperelastic behavior of rubberlike materials.* Abaqus Analysis Users' Manual ver.6.6. **3**: p. 17.5.1-5.

43.   Hu, T., Desai,P., *Characterization of Soft-Tissue Material Properties: Large Deformation Analysis* in *Medical simulation.* 2004, Springer Berlin / Heidelberg. p. 28-37.

44.   Nielsen, P.M.F., Hunter,P.J., Smaill,B.H., *Biaxial testing of membrane biomaterials: Testing equipment and procedures.* Journal of biomechanical engineering, 1991. **113**: p. 295-300.

45.   Timoshenko, S., *Theory of plates and shells.* 1978.

46.   Wan, K., Mai,YW, *Fracture mechanics of a shaft-loaded blister of thin flexible membrane on rigid substrate.* International journal of fracture, 1995. **74**(2): p. 181-197.

47.   Wan, K.-T., Guo,S., Dillard,D.A., *A theoretical and numerical study of a thin clamped circular film under an external load in the presence of a tensile residual stress.* Thin solid films, 2003. **425**(150-162).

48.   Zauberman, H., Berman, E.R., *Measurement of adhesive forces between the sensory retina and the pigment epithelium.* Experimental eye research, 1969. **8**(3): p. 276-83.

49.   Hoferlin, E., Van Bael,A., Van Houtte,P., Steyaert,G., DeMare,C., *The design of a biaxial tensile test and its use for the validation of crystallorphic yield loci.* Modelling Simul. Mater. Sci. Eng., 2000. **8**: p. 423-433.